LEE, HO YOUNG, M.S. Doxorubicin-Induced Cytotoxicity in Rat Myocardial H9c2 Cells: The Roles of Reactive Oxygen Species and Redox Balance. (2017).
Directed by Dr. Zhenquan Jia. 65 pp.

Doxorubicin (Dox) is one of the most potent anti-neoplastic agents approved by the Food and Drug Administration. Its efficacy, however, is limited due to its well-documented cardiotoxic side effect. Since the first observation of this dosage-dependent side effect, the mechanisms and events leading to cardiotoxicity following exposure to doxorubicin have received much attention. However, the exact pathogenesis of Dox-induced cardiotoxicity remains to be elucidated. Although increased production of reactive oxygen species (ROS) from the redox cycling of Dox has been recognized as the primary mechanism of Dox-induced cardiotoxicity, it must be noted that many of the studies supporting the oxidative stress-induced cardiotoxicity hypothesis were conducted with supraclinical drug concentrations. This study examined the effect of clinically-relevant concentrations of Dox on H9c2 rat cardiomyoblasts. Through MTT-reduction cell viability assay, it was determined that exposure of H9c2 cells to Dox concentrations above 0.5 μM for more than 12 hours resulted in significant reduction in cell viability. To verify the role of oxidative stress on the development of cytotoxicity, ROS levels after exposure to low concentrations of Dox (less than 2 μM) were measured. Quantitative measurements of both cellular and mitochondrial ROS levels revealed no significant changes to superoxide presence while exhibiting significant decrease in hydrogen peroxide presence. However, despite the decreased presence of two major types of ROS, the potency of antioxidant responses from the H9c2 cells were found to have significantly

increased. Also, exposure to Dox at clinically relevant concentrations led to significant increase in the gene expressions of vascular cell adhesion molecule 1 (VCAM-1) and intercellular adhesion molecule 1(ICAM-1), two key adhesion molecules that have been implicated in Dox-induced cardiotoxicity. These results suggest that lower concentrations of Dox can stimulate intracellular anti-oxidative response that may thwart intracellular ROS levels required for maintaining of proper cell functions, ultimately leading to redox imbalance and inflammation in cardiomyocytes.

While attempting to further investigate into the specific mode of cell death induced by Dox treatment, it was found that the innate fluorescence of Dox may be potent enough to be recognized by various fluorescence-based detection methods. Dox was found to exhibit fluorescence spectra consisting of a maximum excitation wavelength of 493 nm and a maximum emission wavelength of 592 nm, which were similar to the fluorescence characteristics of common fluorescent markers such as FITC, PI, MitoSOX, and DCF-DA which are widely used to assess cell viability, as well as ROS production. Furthermore, nuclear accumulation of Dox was confirmed by fluorescence microscopy, and spectrofluorometric measurements which detected the cellular uptake of Dox. This suggests that the innate fluorescence of Dox can be a valid probe used for future investigations for the uptake, release and distribution of Dox both *in vitro* and *in vivo*.

Altogether, this study demonstrated for the first time that exposure to Dox at clinically relevant plasma concentrations significantly decreased hydrogen peroxide levels below the basal levels in both intact H9c2 rat cardiomyocytes and in isolated

mitochondria. Cells treated with Dox showed a significant increase in the expression of genes associated with anti-oxidative response and inflammation. Utilizing the intrinsic fluorescence of Dox, it was found that incubation of H9c2 cells with Dox resulted in time-dependent intracellular uptake of Dox. This study may contribute in advancing our understanding of mechanisms responsible for Dox-induced cardiotoxicity and thereby improving the efficacy of Dox, one of the most prominent components of many chemotherapy regimens.

Keywords

CVDs, Cardiotoxicity, Doxorubicin, Clinically-relevant concentrations, H9c2 rat cardiomyoblasts, Redox, ROS, Apoptosis, Necrosis, Inflammation, Fluorescence, Uptake

DOXORUBICIN-INDUCED CYTOTOXICITY IN RAT MYOCARDIAL H9C2 CELLS: THE ROLES OF REACTIVE OXYGEN SPECIES AND REDOX BALANCE

by

Ho Young Lee

A Thesis Submitted to
the Faculty of The Graduate School at
The University of North Carolina at Greensboro
in Partial Fulfillment
of the Requirements for the Degree
Master of Science

Greensboro
2017

Approved by

_____
Committee Chair

Thank you Lord for your blessings for it would not have been possible without You. Thank you to the only love of my life Hyelim for your patience and companionship. Thank you gomo and gomobu for always being the lighthouse in the sea of uncertainties. I could not have persevered through this process without the tremendous support from my families here in the US and in the Republic of Korea. Thank you UNCG Biology Department and thank you everyone at the Jia Lab for their love, friendship, and guidance.

APPROVAL PAGE

This thesis written by Ho Young Lee has been approved by the following committee of the Faculty of The Graduate School at the University of North Carolina at Greensboro.

Committee Chair _____

Committee Members _____

_____

_____
Date of Acceptance by Committee

_____
Date of Final Oral Examination

ACKNOWLEDGEMENTS

I would like to thank my advisor, Dr. Zhenquan Jia and committee members Dr. Amy Adamson and Dr. Paul Steimle for their guidance and support. I would also like to thank the UNCG biology department for all of the support that was necessary for this study.

TABLE OF CONTENTS

Page

LIST OF FIGURES

Page

CHAPTER I

INTRODUCTION

Anthracyclines: An Overview

Anthracyclines were first introduced in the 1960's and have remained as a mainstay of chemotherapy, treating patients suffering from leukemias, lymphomas, breast, stomach, ovarian, and lung cancers. Anthracyclines contribute to the high survival rates of 70 and 75% in pediatrics and breast cancer, respectively [2].

Doxorubicin is a member of anthracycline antitumor antibiotics that are commonly used to treat a wide variety of cancers [3]. Its anti-malignancy effect is modulated by the ability of doxorubicin to intercalate between the base pairs of double-stranded DNA, thereby inhibiting DNA topoisomerase II (Topo II) activity. The inhibition of Topo II activity compromises the structural integrity of DNA, inducing a double stranded break in DNA, halting the DNA replication process, which is instrumental for rapidly proliferating tumor cells. Inhibition of Topo II also leads to activation of p53 and the production of

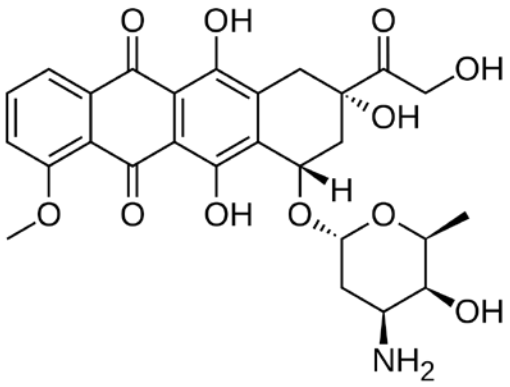

Figure 1. Structure of Doxorubicin.

Dox is comprised of a tetracyclic ring with quinone and hydro quinone groups along with methoxy substituent side chain grou p and a carbonyl group[1].

several proteins that promote cell cycle arrest and apoptosis [4]. Additionally, Dox inhibits the natural DNA repairing mechanism of topoisomerase II by stabilizing the formation of DNA-enzyme intermediate which consists of 5'-phosphoryl end of the nicked DNA covalently bonded to the tyrosine residues of topoisomerase II. This eventually hinders DNA rejoining process that follows. Such DNA damage induced by Topoisomerase II results in a growth arrest in the G1 and G2 phases and apoptosis [5].

Pharmacokinetics of Doxorubicin

Early investigation using the innate fluorescence of Dox to follow the cellular uptake revealed subsequent localization of Dox in the nucleus [6]. Proceeded studies have confirmed that Dox is able to cross the cell membrane via passive diffusion [1, 7]. While the distribution half-life of Dox ranges from 3 to 5 minutes, the terminal half-life of Dox of 24 to 36 hours indicates quick uptake and slow elimination of Dox by target tissues. Such kinetics results in intracellular concentration of Dox being 10 to 500-fold higher than extracellular environment. Nuclear levels of Dox are found to be higher than cytoplasmic Dox level by 50-fold with concentrations up to 340uM. This suggests that Dox is capable of intercalating at every fifth base pair on the DNA strand [8].

The lipophilic characteristic of Dox along with its DNA intercalating property allow Dox to quickly penetrate tissues and prolong its presence within the target tissue. This phenomenon is clinically observed as a rapid drop in plasma Dox levels in patients' blood is seen while Dox levels in bone marrow and white blood cells become 200-500 times higher than that found in blood [8].

The biotransformation of Dox occurs in the liver as it is metabolized to doxorubicinol by aldo-keto reductase. Doxorubicinol, a dihydrodiol derivative which maintains Dox's antitumor activity, can be further metabolized by cytochrome P450 (CYP) reductase to cleave the glycosidic bond and release aglycone metabolites that are believed to be involved in the development of cardiotoxicity. Both metabolites are excreted extensively into the bile by various transporters including P-glycoprotein [9]. Half of the excreted drug is in the bile, usually being excreted within 5 to 7 days of treatment, while only 5 to 12% of Dox is found in urine during the same time period. After 24 hours, 10 to 20% of Dox is excreted in feces, and 50% after 150 hours [10].

Doxorubicin-Induced Cardiotoxicity

Despite its extensive utilization in clinical setting, the efficacy of doxorubicin's therapeutic effect is limited by cumulative dose-dependent cardiotoxicity that may, ultimately, result in heart failure [11]. Since the 1970s, cumulative dose-dependent cases of heart failures have been continuously observed in cancer patients who underwent anthracycline chemotherapy, indicating possible anthracycline-induced cardiotoxicity [12]. Two major types of cardiotoxicity have been observed in clinical settings – acute and chronic. Acute cardiotoxicity, characterized by arrhythmias and a reversible decrease in ventricular output [11], was found to be occurring during and within 2-3 days of administration with an incidence of approximately 11% [13, 14]. Chronic cardiotoxicity is characterized by mostly irreversible decrease in ventricular output with a direct relationship to the cumulative dose of doxorubicin [15]. Clinical analysis of doxorubicin-

treated patients revealed that 4% of patients exhibited signs of cardiotoxicity when cumulative doxorubicin dose was 500 – 550 mg/m^2. Cumulative doxorubicin dose of 551 – 600 mg/m^2 increased the incidence to 18% while cumulative dose exceeding 600 mg/m^2 resulted in incidence of 36% [16].

Mechanism of Doxorubicin Cardiotoxicity Remains Unclear

Although medical advancements in terms of diagnosis, treatment, and prevention along with improved understanding of cancer pathogenesis have greatly increased cancer survival rates across various parameters; the risk of anthracycline-induced cardiotoxicity has not been abated largely due to lack of clear understanding of the mechanisms through which doxorubicin causes irreversible myocardial injury. The following are several mechanisms of doxorubicin cardiotoxicity have been proposed and have received much attention : increased oxidative stress [14, 17], decreased expression of antioxidants [17, 18], ROS-induced inflammation, and mitochondrial dysfunction [19].

Evidenced by increased generation of reactive oxygen species, oxidative stress has been implicated to doxorubicin-induced cardiotoxicity leading to heart failure. Although heart failure, in general, is multifactorial, substantial evidence has suggested that a failed defense against ROS resulting in oxidative stress is one of the primary underlying causes of heart failure. Increased lipid peroxidation was observed in congestive heart failure patients [20] and animal models of heart failure also detected superoxide anion and hydrogen peroxide [21, 22]. It is suggested that the quinone form of doxorubicin can accept an electron to produce the semiquinone form of doxorubicin.

Incomplete reduction of molecular oxygen can cause the redox cycling of doxorubicin as the semiquinone form is oxidized back to the original quinone form. During this process, the molecular oxygen becomes incompletely reduced and becomes a superoxide anion radical ($O_2^{\bullet-}$) [23]. Superoxide radicals, considered as primary reactive oxygen species (ROS), then undergo further metabolism and interact with other molecules to generate secondary ROS such as hydrogen peroxide (H_2O_2) and highly-reactive hydroxyl radicals ($^{\bullet}OH$) [24]. ROS are often characterized by their capability to bring incredible amounts of both discriminant and indiscriminate damage to biomolecules including protein, lipids, and nucleic acids. The interaction between ROS and biomolecules often result in chain reactions that lead to the generation of electrophiles that are detrimental to host cells' health [25].

In addition to inducing direct cellular damage, another way ROS may contribute to inducing heart failure is by inducing inflammation. Although inflammatory responses are vital part of the innate immunity, these non-specific immune responses should be temporary as extended or chronic inflammation may cause tissue injury leading to various diseases [26]. ROS-induced inflammation has been reported to play an important role in cardiovascular diseases [27-30]. ROS signaling is involved in various aspects of immune response against environmental chemicals. In cell-mediated immunity, T-lymphocyte activation was found to be enhanced by presence of ROS [31]. In primary immune response, massive production of ROS, also known as oxidative burst, is observed in activated neutrophils and macrophages as an inflammatory response against

environmental pathogens. However, the same process can also induce tissue injury as ROS released by neutrophils may indiscriminately harm uninjured cells. Additionally, ROS have been implicated as an important messenger involved in the activation of NFκB (also known as p65/50), a ubiquitously expressed transcription factor involved in inflammatory response [32]. Although ROS has not been shown to directly activate the cytosolic NFκB molecules, it does so via its involvement with tumor necrosis factor (TNF) and interleukin-1 (IL-1) [33]. Activation of NFκB has shown to induce expression of various inflammatory mediators such as monocyte chemotactic protein 1 (MCP-1), interleukin 6 (IL-6), IL-8, E-selectin, intracellular adhesion molecule-1 (ICAM-1), and vascular cell adhesion molecule-1 (VCAM-1) [34-36]. Inflammatory mediators, particularly IL-2 and TNF-α, have been implicated in doxorubicin-induced cardiotoxicity [37]. Since cardiomyocytes express functional receptors for these cytokines, the release of these cytokines has been suggested to be involved in dilated cardiomyopathy observed in patients treated with doxorubicin [37].

Although ROS are predominantly implicated in causing cell damage, recent studies have provided new insights into ROS as having major physiological roles in cell signaling and signal transduction pathways involved in cell growth, differentiation [34, 38, 39], and, as previously mentioned, in host defense mechanism by acting as a component of the killing response of immune cells to invasion by infectious agents [40]. ROS-mediated redox signaling pathways found in cells under normal physiological conditions explains the capability of many types of cells to produce endogenous ROS. Some of the signaling mechanisms involving transcription factors, protein tyrosine

phosphatases, selective classes of kinases, and JNK MAPK signaling pathways respond to this temporary imbalance in redox homeostasis [32, 38]. It is currently understood that ROS is involved in both pathological mechanisms and normal physiological functions, and this double-edged characteristic of ROS further highlights the significance in fully understanding its potential mechanisms linking doxorubicin exposure to cardiotoxicity.

The Selective Toxicity of Doxorubicin to the Heart

Several factors are believed to contribute as to why doxorubicin selectively damages the myocardium, resulting in cardio-specific toxicity. Firstly, myocardium is highly oxygenated, favoring ROS and reactive nitrogen species (RNS) production. Specifically, myocardial cells of the left ventricle (LV) receive an oxygen-rich supply of blood. Interestingly, one of the main characteristics of Dox-induced cardiotoxicity is dysfunctional LV. Additionally, due to their role in oxidative phosphorylation, cardiomyocytes have been found to be rich in mitochondria, making at least 30% of the cell's volume [41]. The abundant presence of mitochondria and the continuous production of ATP via electron transport chain (ETC), a process known to have potential for ROS production, favors redox cycling of Dox to generate semiquinone radicals and ROS/RNS. Thirdly, previous studies have implicated that Dox has a high affinity for cardiolipin, an acidic phospholipid molecule found primarily in the inner mitochondrial membrane. The interaction between Dox and mitochondrial cardiolipin is thought to be involved in the Dox-induced cardiotoxicity [42]. There is accumulating evidence that suggests that the oxidation of cardiolipin due to oxidative stress leads to release of

cytochrome c, a critical event in apoptosis. Lastly, cardiomyocytes have relatively low expression of ROS-detoxifying enzymes such as superoxide dismutase (SOD), glutathione peroxidase (GPX), peroxiredoxins, thioredoxin reductase, catalase, and non-enzymatic antioxidant molecules [43-45].

With high oxidative metabolism coupled with poor reserve of antioxidants in cardiomyocytes, the hypothesis of increased oxidative stress due to redox cycling of the quinone moiety of doxorubicin leading to production of ROS has often been considered as the primary mechanism behind doxorubicin-induced cardiotoxicity. However, it must be emphasized that many of the past studies supporting the oxidative stress-induced cardiotoxicity hypothesis were conducted under supraclinical drug concentrations that were, in some cases, several log orders higher than that observed in clinical settings [46-55]. It has been suggested that clinically relevant plasma concentrations of doxorubicin range from 11 nM to 2 μM [56]. The initial observation of doxorubicin concentration in blood plasma of cancer patients under bolus administration was approximately 2.78 μM with terminal half-life of 39.5±10.4 hours [57]. However, plasma concentrations of those who underwent prolonged continuous infusion of doxorubicin (96 hours) was lower as it was observed to be approximately 21nM with slighter longer half-life of 44.6±8.5 hours. Therefore, it is important to note that the results from previous studies involving supraclinical concentrations of doxorubicin may not accurately reflect the mechanism of doxorubicin-induced cardiomyopathy at normal physiological conditions.

Proposed Study

The primary goal of this study is to elucidate the underlying mechanisms leading to Dox-induced cytotoxicity of H9c2 rat cardiomyoblasts following exposure to clinically-relevant concentrations of Dox. Based on the preliminary data observed previously, the hypothesis of the thesis was that H9c2 cells, when exposed to clinically-relevant concentrations of Dox, initiate antioxidative response that inadvertently lower ROS presence below the basal intracellular ROS level required for maintaining of proper cell functions, ultimately leading to redox imbalance and cell death.

In accordance with the hypothesis, the first objective of this study was to assess the cytotoxicity induced on the H9c2 rat cardiomyoblasts by clinically-relevant concentrations of Dox. Upon determination of Dox concentration and exposure time needed to induce cytotoxicity in H9c2 cells, cells' redox balance state was examined by analyzing the readiness and potency of the cells' antioxidative response and quantitatively measuring the ROS presence. The second aim was to investigate the innate fluorescence of Dox in hopes to validate the practicality in utilizing the fluorescence capability of Dox as a possible tool for future investigations of Dox-induced cytotoxicity.

CHAPTER II

MATERIALS AND METHODS

Chemicals and Materials

Dulbecco's Modified Eagle's Medium (DMEM), penicillin/streptomycin, fetal bovine serum (FBS), and trypsin were purchased from Gibco, Invitrogen. 2-Cyano-3, 12-dioxooleana-1,9-dien-28-imidazolide (CDDO-Im) was purchased from Toronto Research Chemicals, Inc. Reduced glutathione, oxidized glutathione, o-phthalaldehyde (OPT), NADPH, MTT, and BSA were purchased from Calbiochem. Doxorubicin and hydrogen peroxide were purchased from Sigma. Tissue culture flasks (75 cm2) and 12-, 24-, 48-, and 96-well plates were purchased from Greiner Bio-One and Corning.

Cell Culture

H9C2 *Rattus norvegicus* myocardial cell line was cultured in Dulbecco's Modified Eagle's Medium with following components: 1% Penicillin Streptomycin (P/S) and 10% Fetal Bovine Serum (FBS). 75cm^2 Cellstar® cell culture flasks from Greiner Bio-One (Catalog number: 658170) were used. The flasks containing the H9C2 cells were maintained in a humidified environment with temperature of 37°C and 5% CO_2. DMEM was renewed every 2 to 3 days, and the cells were passaged at 80% confluency.

Doxorubicin Treatments and Cell Extraction Preparation

H9C2 rat cardiomyocytes were exposed to Dox in both time-dependent (0, 1, 3, 6, 12, 24 hours) and concentration-dependent (0, 0.1, 0.5, 1, 2, 4μM) manners in DMEM supplemented with 10% FBS and 1% P/S. At the termination of the treatments, media were aspirated, and cells were washed twice with sterile phosphate-buffered saline (PBS) solution to remove excess trace of DMEM. Cell detachment was carried out by applying 4~5 mL of trypsin. After 3~5 minutes of incubation at 37°C, fresh ice-cold DMEM (10%FBS, 1% P/S) was added to neutralize trypsin activity. Resulting mixture underwent an initial centrifugation at 1,000 RPM for 7 minutes at 4°C. Cells were then resuspended in 1 mL of PBS and centrifuged at 5,000 RPM for 5 minutes at 4°C. The resulting pellet was resuspended in 300 μL KH_2PO4/K_2HPO4 buffer (pH 7.4) containing 2 mM EDTA. Cells were then sonicated during three cycles consisting of 12 seconds of sonication and 5 seconds of rest to prevent denaturing of cellular protein due to heat. The resulting mixture was centrifuged at 13,000 RPM for 10 minutes at 4°C. Supernatants were collected and stored on ice for quantitative measurement of cellular GSH content, NQO1, and GST activity.

Total Protein Quantification Assay

790 μL of deionized water, 200 μL of Bio-Rad Protein Assay Dye Reagent Concentrate® (Cat #500-0006) and 10 μL of cell extraction lysate was added and vortexed. Using Beckman Coulter DU800 spectrophotometer, absorbance at 595 nm was measured. The observed absorbance reading of the samples were compared to the

absorbance reading of a 1.48 mg/ml Bovine Serum Albumin (BSA) standard to determine the total protein concentration of the samples.

Cellular Glutathione (GSH) Assay

10 μL of cell extraction lysate samples were mixed with 12.5 μL of 25% metaphosphoric acid (HPO_3) and 37 μL of 0.1M sodium phosphate buffer (pH 8.0). The mixtures were incubated for 10 minutes at 4°C followed by centrifugation at 13,000 RPM for 5 minutes at 4°C. 40 μL of the resulting supernatant were incubated with 1.86 mL of 0.1M sodium phosphate buffer and 100 μL of o-phthalaldehyde (OPT) for 15 minutes at room temperature shielded from light. After the 15-minute incubation, samples were transferred to black 96-well plate and the intensity of the fluorescence was measured at an excitation wavelength of 350 nm and an emission wavelength of 420 nm. The observed fluorescence readings of the samples were compared to fluorescence of a 1.25 μg/ml GSH standard to determine the total GSH.

Cellular NADPH Quinone Oxidoreductase-1 Activity Assay

NQO1 reaction mix was prepared immediately prior to measurement by mixing 12 mL of 50 mM Tris-HCl buffer (pH 7.5, 0.08% Triton X-100), 36 μL of 50 mM Nicotinamide adenine dinucleotide phosphate (NADPH), and 48 μL of Dichlorophenolindophenol (DCPIP). 4 μL of sample and 2.8 μL of dimethyl sulfoxide (DMSO) were mixed with 696 μL of the reaction mix. The NQO1 enzymatic activity, the rate at which DCPIP is being reduced by NQO1, was determined by measuring

absorbance at 600 nm for three minutes in 20 second intervals using the DU800 spectrophotometer.

Flow Cytometric Analysis for Cell Death

Following a 24-hour treatment of H9C2 cells with appropriate concentrations of Dox, the cells were trypsinized and centrifuged at 1,000 RPM for 7 minutes at 4°C. The resulting pellet was suspended in appropriate volume of PBS in order to induce target cell concentration range of 1 x 10^6 and 1 x 10^7cells per mL and incubated with 2 μg/ml Annexin V-FITC and 2.5 μg/ml PI for 30 min at 4 °C. The cells were analyzed using Guava® easyCyte Flow Cytometer. easyCyte flow cytometer used blue laser with excitation wavelength of 488 mm and three distinct filters for detection (525/30 nm, 583/26 nm, 695/50 nm).

MTT Cell Viability Assay

H9C2 cells were grown to about 70% confluence in a 24-well Costar® cell culture plate. Cells were exposed to appropriate concentrations of Dox and incubated in humidified environment with temperature of 37°C and 5% CO_2 for target time periods. At the termination of the Dox treatment, the media were replaced with 500 μL/well of DMEM (10% FBS, 1% P/S) supplemented with 3-(4,5-dimethylthiazol-2-yl)-2,5-diphenyltetrazoliμM bromide (MTT) reagent (final concentration of 0.2 mg/mL) and incubated for 1.5 hours in humidified environment with temperature of 37°C and 5%

CO_2. After the 1.5-hour incubation, media was carefully aspirated, and 200 µL of 7:3 dimethyl sulfoxide to water dissolving solution was added to solubilize the resulting formazan crystals. Cell viability was determined by quantifying the amount of dissolved formazan by analyzing absorbance at 570 nm using the Bio-Tek® microplate reader.

LDH Cell Viability Assay

H9C2 cells were cultured to approximately 90% confluency in a 24well Costar® clear cell culture plate using non-phenol red 10% FBS DMEM. The cells were then treated with appropriate concentrations of Dox in 10% FBS DMEM for 24 hours. Media from each well was collected into 1.5 mL microcentrifuge tubes and centrifuged for 5 minutes at 13,000 rcf. The resulting supernatant was collected for spectrophotometric analysis.

Glutathione S-Transferase (GST) Assay

GST reaction mix was first prepared with 15 mL of 0.1 M phosphate buffer (pH 6.5), 45 mg of BSA, 300 µL of 50 mM 2,4-Dinitrochlorobenzene (CDNB), and 150 µL of 100 mM GSH. The mixture was transferred to a clear cuvette into which 15 µL of cell extraction lysate sample was added. Formation of CDNB-GSH conjugate was quantitatively measured by observing the absorbance at 340 nm for 5 minutes in 30 second intervals.

Quantitative Real Time Polymerase Chain Reaction (qRT-PCR)

H9C2 cells were grown to approximately 80% confluence and treated with appropriate concentrations of Dox for 24 hours. TRIzol® Reagent (ambion® Ref. number: 15596-018) was used to extract total RNA from the cells. Protocol for RNA isolation provided by the manufacturer (Life Technologies) was used. Using Nanodrop 2000® (Thermo Scientific), the purity and concentration of the isolated RNA was determined. For reverse transcription of the isolated RNA, 2 μL of RNA, 1.25 μL of deoxynucleotide triphosphates (dNTP) solution, 1.25 μL of random primers, 0.625 μL of Moloney Murine leukemia virus reverse transcriptase (MMLV RT), was added to 14.875 μL of diethyl pyrocarbonate-treated (DEPC) water to a total volume of 25 μL. The resulting complementary DNA was diluted (1:9 ratio with DEPC water) and added to the Life Technologies™ Power SYBR® Green PCR Master Mix and rat/mouse primers sets (forward and reverse) for *NQO1*, Glutamine-cysteine ligase catalytic subunit (*GCLC*), vascular cell adhesion protein (*VCAM*), and intercellular adhesion molecule (*ICAM*). To normalize the expression of the target genes, the target gene expressions were compared to that of glyceraldehyde 3-phosphate dehydrogenase (*GAPDH*) gene expression. A total of 40 cycles was performed for each run as follows: 95ºC for 15 seconds, 58ºC for 1 minute, and 60ºC for 15 seconds. The comparative threshold cycle C_T method was used to quantify gene expressions. The following description details the nucleic acid sequence of the forward and reverse primers used: *ICAM* forward primer sequence(5'-CAATTTCTCATGCCGCACAG-3') *ICAM* reverse primer sequence (5'-AGCTGGAAGATCGAAAGTCCG-3') *VCAM* forward primer sequence (5'-

TGAACCCAAACAGAGGCAGAGT-3') *VCAM* reverse primer sequence (5'-GGTATCCCATCACTTGAGCAGG-3') *GCLC* forward primer sequence (5'-AACACAGACCCAACCCAGAG-3') *GCLC* reverse primer sequence (5'-TGGCACATTGATGACAACCT-3') *NOQ1* forward primer sequence (5'-CACGCATATACCCGCTACCT-3') *NQO1* reverse primer sequence (5'-CCAGAGTGTTCATTCGAGCA-3') *GAPDH* forward primer sequence (5'-GGAGAAACCTGCCAAGTATGA-3') *GAPDH* reverse primer sequence (5'-TACTCCTTGGAGGCCATGTA-3')

Cellular Reactive Oxygen Species (ROS) Detection Assay

Complete phosphate buffered saline (cPBS) solution was first prepared by supplementing phosphate buffered saline (PBS) solution with 0.5 mM $MgCl_2$, 0.7% mM $CaCl_2$, and 0.1% glucose. An automatic air pump was used to saturate the prepared cPBS with oxygen for 30 minutes at 37ºC. H9c2 cells, grown to 90% confluence, were harvested and suspended in the oxygen-enriched cPBS. The cells were counted and diluted to 2 x 10^6 cells and aliquoted into 1.5 mL Eppendorf® microcentrifuge tubes. 5 µL of luminol and 5 µL of horseradish peroxidase (HPR) was added into the micro centrifuge tubes with cells. The suspension was mixed, and luminescence was measured in real time using Berthold Biolumat LB 9505 luminometer. The intensity of the luminescence of treated cells will be compared to that of an untreated control.

Fluorescence Microscopic Imaging

H9c2 rat cardiomyoblasts were seeded into Corning 100 mm TC-treated culture dishes. The cells were then exposed to target concentrations of Dox in 10% FBS DMEM for 24 hours. At the termination of the treatments, cells were rinsed twice with sterile PBS and 5 mL of PBS was added. An EVOS Floid cell imaging system (Thermo Fisher) was used to capture images using bright field, GFP, RFP capture options as well as to generate an overlay of images from the bright field and the RFP imaging options.

Fluorescence Spectrometric Characteristics of Doxorubicin

To realize the fluorescence spectrometric characteristics of Dox, Varian Cary 50 Bio UV Vis Spectrometer was used to observe the emission and excitation spectra of Dox. 10 uL of 10 mM Dox was added to 3 mL of PBS to observe the fluorescence spectra of Dox.

Fluorescence-based Analysis of Cellular Uptake of Doxorubicin

H9c2 rat cardiomyoblasts were seeded into PerkinElmer Viewplate- 96 Black, Optically clear bottom tissue culture plates. Upon reaching 70% confluency, cells were exposed to the appropriate concentrations of Dox for up to 12 hours in 10% FBS- and 1% P/S-supplemented DMEM. At the termination of Dox exposure, all media were carefully aspirated, and cells were washed twice with 200 uL of sterile PBS. 100 uL of sterile PBS was added, and the Bio-Tek® Synergy2 microplate reader was used to analyze the fluorescence of intracellular Dox. Bandpass filters permitting excitation wavelength

range of 490/20 nm and emission wavelength range of 590/35 nm were used. To further increase the gain and sensitivity for fluorescence intensity, 510 nm dichroic mirror was applied.

Mitochondrial Isolation and Mitochondrial Lysate Preparation

H9c2 rat cardiomyoblasts were cultured until 80% confluency. Cells were collected using trypsin and rinsed one with PBS. The cell pellet was resuspended in 5 mL sucrose buffer consisting of 0.25 M sucrose, 1 mm EGTA, 10 mM HEPES, and 0.5% BSA (pH 7.4). Using a Dounce homogenizer on ice, the cell pellet was homogenized until methyl blue staining of the homogenate indicated rupturing of most of the cells. Differential centrifugation was implemented to separate the proportion of the homogenate containing only mitochondria. The homogenate was then centrifuged at 10,000g at 4°C for 10 minutes to produce mitochondrial pellet. The homogenate was then resuspended in 1 mL of sucrose buffer without BSA. For mitochondrial ROS analysis, the resuspended pellets were stored in -80°C. For mitochondrial antioxidant quantification and phase 2 enzyme activity level investigations, the mitochondrial pellet was lysed via sonication immediately followed by mitochondrial protein concentration analysis.

Mitochondrial ROS Detection Assay

For detection of superoxide production in isolated mitochondria, the reaction mixture contained 0.5 mg/ml of isolated mitochondria in 1 ml of air-saturated mitochondrial respiration buffer consisting of 70 mM sucrose, 220 mM mannitol, 2.5

mM KH_2PO_4, 2.5 mM $MgCl_2$, 2 mM HEPES, 0.5 Mm EDTA, and 0.1% BSA (pH 7.4). After the addition of various concentrations of Dox, 6 mM succinate and lucigenin was added to initiate the chemiluminescence response. The resulting real-time CL responses were observed for 30 minutes.

For detection of hydrogen peroxide production in isolated mitochondria, the reaction mixture contained 50 ng/ml (5 uL of 1 mg/mL suspension of isolated mitochondria) of isolated mitochondria in air-saturated mitochondrial respiration buffer pre-warmed to 37°C. After the addition of various concentrations of Dox, succinate was supplemented to final concentration of 5 mM. To initiate the CL response, 5 uL of 2 mM luminol along with 5 uL of 2 mg/mL Horseradish Peroxidase (HRP) was added to the reaction mixture. The resulting real-time CL responses were observed for 30 minutes.

CHAPTER III

RESULTS

Dox-induced Concentration-dependent and Time-dependent Cytotoxicity

In the current study, the cellular toxicity of rat H9c2 cardiomyoblasts upon exposure to different concentrations of Dox was first assessed by quantitatively measuring the reduction of MTT. H9c2 cells, seeded on clear 24-well cell-culture plates, were exposed to 0, 0.1, 0.5, and 1 µM of Dox for up to 24 hours. After two PBS rinses, the cells were incubated in MTT solution for 1.5 hours, resulting in the formation of formazan crystals. Formazan crystals were dissolved using 1 mL of dissolving solution consisting of 7:3 ratio of DMSO and water. The resulting solution containing dissolved formazan crystals was analyzed for absorbance at 570nm as an indication of cell viability.

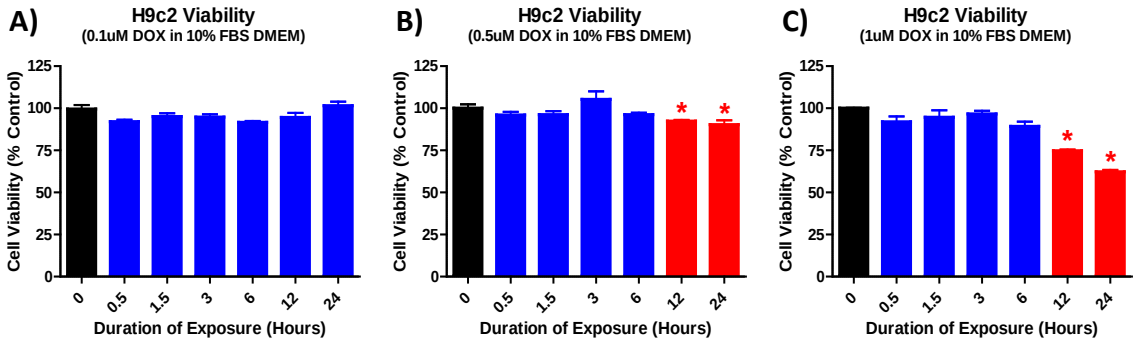

Figure 2. Time and Dosage Dependent Data on Dox-Induced Cytotoxicity in H9c2 Cells.

H9c2 cells were exposed to various concentrations of Dox for up to 24 hours. After two PBS rinses, the cells were incubated in MTT solution for 1.5h hours, resulting in formation of formazan crystals. The formazan crystals were dissolved using DMSO and absorbance at 570nm was observed as indication of cell viability. *All data represent mean ± SEM. *P<0.05 in comparison to the control group (n=4).*

Figure 2 depicts time-dependent cytotoxicity of Dox on H9c2 cardiomyoblasts. Incubation with 0.5 µM and 1 µM of Dox caused significant cell death after 12 hours ($P < 0.05$). These results from time-dependent observations were further corroborated by results in a dose-dependent observation as represented in figure 3-A. MTT analysis of H9c2 cells treated with various concentrations of Dox for 24 hours caused significant toxicity starting at 0.5 µM Dox. It is important to note that the Dox concentrations (0.1-2 µM) used in this study is clinically plasma relevant to humans since clinically relevant plasma concentrations of doxorubicin have been reported to be ranging from 11 nM to 2 µM in human [56, 57]. To further confirm the cytotoxicity of Dox in H9c2 cells, Dox-induced cytotoxicity was assayed by LDH release. As shown in figure 3-B, upon exposure to 0, 0.1, 0.5, 1, and 2 µM of Dox for 24 hours, Dox, only at 2 µM, significantly induced LDH release compared to control ($P < 0.05$).

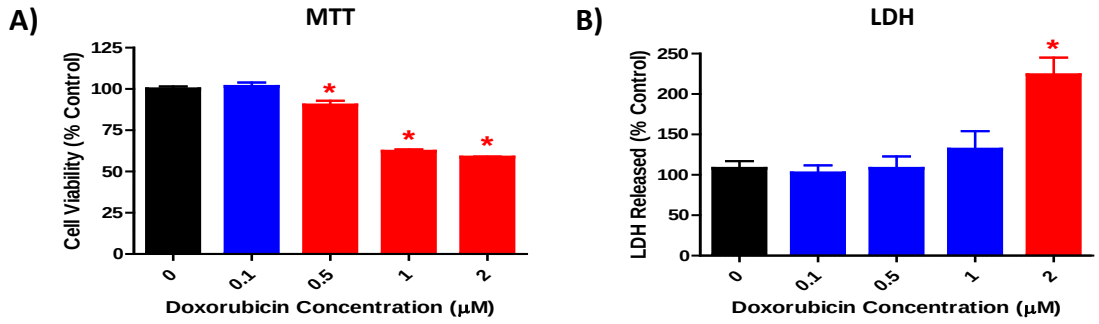

Figure 3. Dosage Dependent Dox Treatment For 24 Hours Decreases Overall Cell Viability of H9c2 Cells.

(A) H9c2 cells were exposed to Dox concentrations up to 2uM for 24 hours. Cells were incubated with MTT solution for 1.5 hours, resulting in formation of formazan crystals. The formazan crystals were dissolved using DMSO and absorbance at 570nm was observed as indication of cell viability. (B) H9c2 cells were exposed to Dox concentrations up to 2uM for 24 hours in phenol red-free media. Supernatant of the samples were collected for absorption observation at 340 nm as indication of the amount of LDH released. *All data represent mean ± SEM. *P<0.05 in comparison to the control group (n=4).*

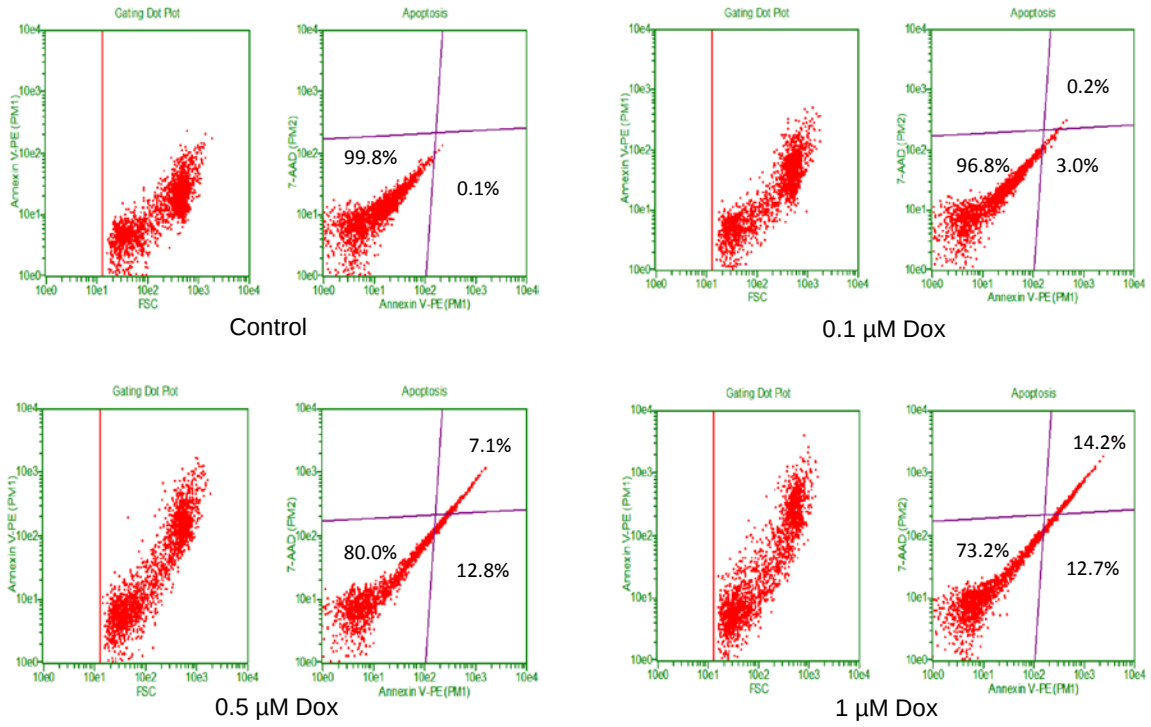

Figure 4. Innate Dox Fluorescence Produces Misleading Results.

H9c2 cells were exposed to various concentrations of Dox for 24 hours. Cells were collected and immediate analysis of the cells using flow cytometer was conducted. Although there were no trace dyes used, analysis via flow cytometer showed significant shift across various parameters falsely indicating concentration-dependent increase in number of cells that are apoptotic and necrotic.

Analysis of Dox-induced Cell Death and Detection of Interference by the Innate Fluorescence of Doxorubicin

In effort to determine specific modes of cell death associated with Dox cytotoxicity, flow cytometric analysis using FITC-labelled annexin V and propidium iodide (PI) as fluorescence markers of apoptosis and necrosis, respectively, was performed according to details provided in the "Materials and Methods." During apoptosis, phosphatidylserine (PS) is known to translocate from the inner membrane to the outer membrane of the phospholipid bilayer of cell membrane. Such process allows

PS-FITC conjugation that leads to emission of green fluorescence. PI is known to utilize compromised membrane integrity of necrotic cells to bind to DNA of the cells. Thus, cells negative for both FITC Annexin V and PI are considered viable cells with intact membrane. Apoptotic cells will stain Annexin V positive and PI negative, while cells that are positive for both FITC Annexin V and PI detection are considered to be necrotic. However, as shown in figure 4, cells exposed to Dox concentration as low as 0.1 µM without incubation with any FITC conjugate of Annexin V marker showed increased shift towards FITC green fluoresce intensity compared to control. These results suggested that Dox has its own innate fluorescent that may overlap the emission range with FITC and thus affects FITC-Annexin-V Staining assay.

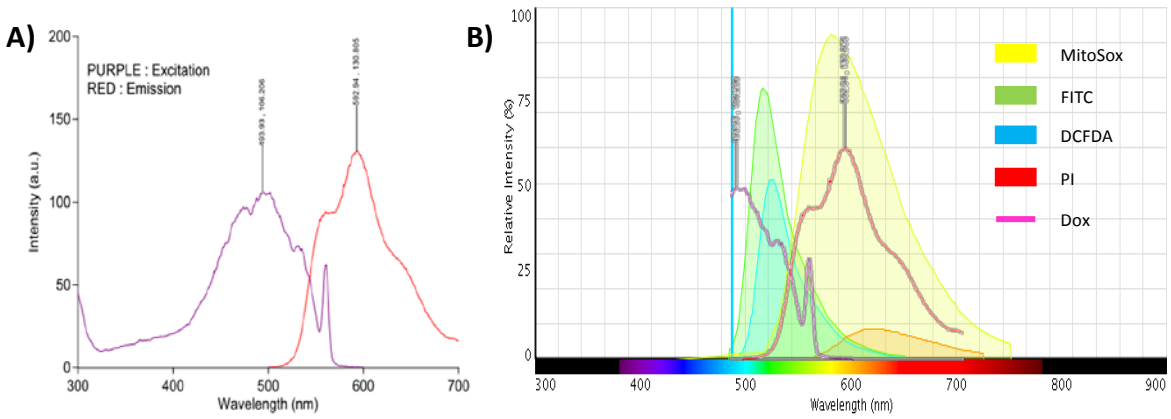

Figure 5. Characteristics of Innate Dox Fluorescence and An Overlay of Emission Spectra of Dox and Various Fluorophores Previously Used in Analyzing Cytotoxicity of Dox.

(A) Dox in PBS was analyzed using a fluorimeter. Excitation peak of 493nm and emission peak of 592nm was observed. (B) The overlay of emission spectra shows overlap between Dox and fluorescent markers commonly used to analyze ROS production and cell viability.

Characterization of Innate Fluorescence of Doxorubicin

To characterize the innate fluorescence property of Dox, 10 µL of 10 mM Dox dissolved in DMSO was added to 3 mL of sterile PBS. The solution was then analyzed using a Cary Eclipse Fluorimeter. As shown in figure 5-A, Dox displays a maximum excitation peak located at 493 nm and a maximum emission peak at 592 nm. Dox exhibited a broad emission spectrum that ranged from 540 nm to 630 nm that produced a relative intensity greater than 50%. Further investigation into the fluorescence spectra of other commonly used fluorochromes including FITC, PI, DCF-DA and MitoSOX showed that Dox's inherent fluorescence range was broad enough overlap with several emission spectra of these fluorescent probes quite commonly used in analyzing various biological systems (Fig. 5-B). For example, as shown in figure 5-B, the emission spectrum of Dox was most similar to that of MitoSOX, a fluorescent dye commonly used as indicators of mitochondrial superoxide presence. Propidium iodide (PI), a widely used indicator of necrosis, was found to have its entire emission range within that of Dox. Although the maximum emission peaks of FITC and DCFDA were well beyond the emission wavelength range of Dox, there were some overlapping of emission range with Dox (Fig. 5-B). DCFDA, as a chemically reduced form of fluorescein, has been widely used as an indicator for ROS, mainly hydrogen peroxide in the cells.

Cellular Uptake of Doxorubicin

Previously shown in figure 5-A, Dox possesses fluorescence capability that was depicted to have an excitation wavelength at 493 nm and an emission wavelength at 592

nm, which allows it to be easily identified through spectrofluorometry, flow cytometry, and/or fluorescence microscopy. This same feature can be very useful for studying the cellular uptake of Dox by H9c2 cells. To do so H9c2 cells were first treated with various concentration of Dox. Cells were then washed two times with PBS (pH 7.4) to remove the excess Dox for the uptake assay.

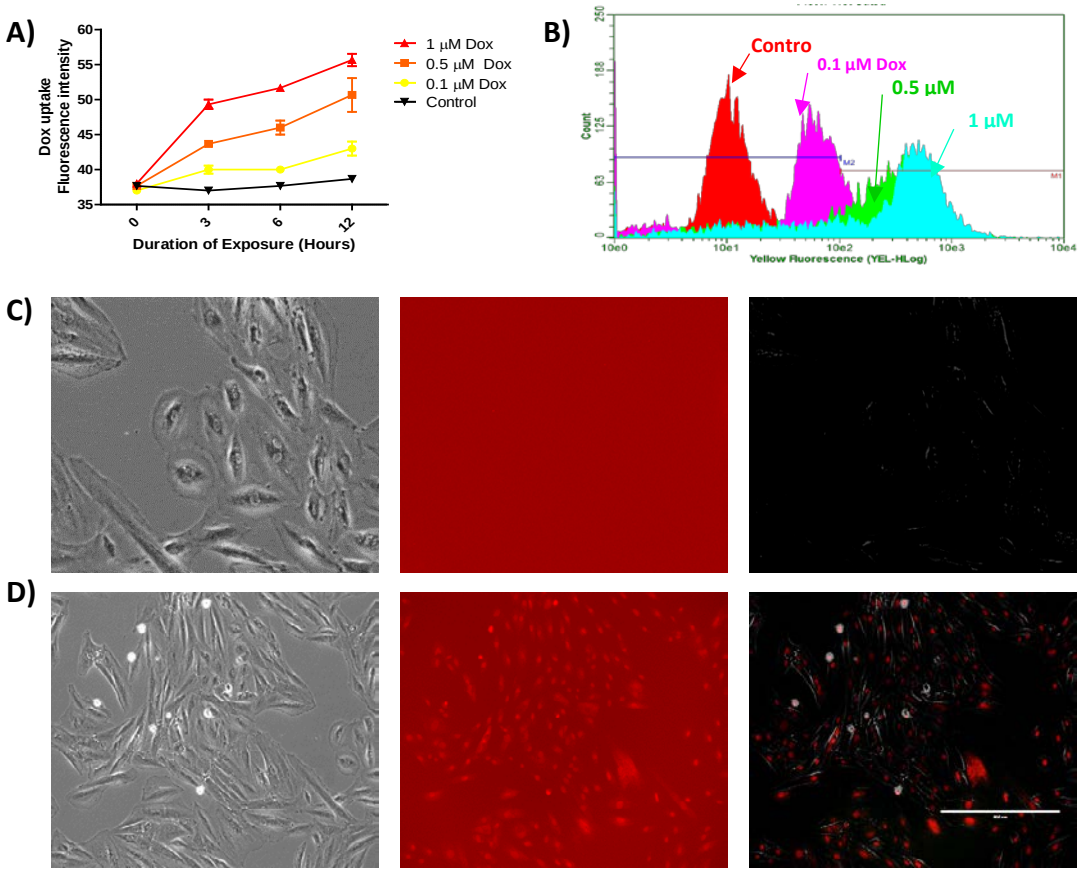

Figure 6. Cellular Uptake of Dox.

H9c2 cells were exposed to various concentrations of Dox for up to 12 hours (A) and 16 hours (B). Cells were collected, rinsed twice with sterile PBS, and resuspended in sterile PBS. Fluorescence was analyzed by Bio-Tek Synergy 2 microplate reader (A), easyCyte flow cytometer (B) and EVOS fluorescence microscope in 10X magnification (C: 0uM Dox exposure, D: 10uM Dox 1hr exposure, Bright field[left], RFP[middle], and BF & RFP overlay[right]). *In Panel A, all data represent mean ± SEM. *P<0.05 in comparison to the control group (n=3).*

As shown in figure 6-A, Dox was taken by cells in both time- and dose-dependent manners. The higher fluorescence intensity of Dox was found after incubating the cells with doxorubicin for 12 hours. Comparable results were observed using flow cytometry studies as emission at the yellow fluorescence with the wavelength bandwidth of 583/26 nm exhibited a concentration-dependent shift compared to the control group (Fig. 6-B). Intracellular uptake of Dox was further identified by visualization under a fluorescence microscope with the excitation wavelength bandwidth of 531/40 nm and emission wavelength bandwidth of 593/40 nm (Fig. 6-C&D).

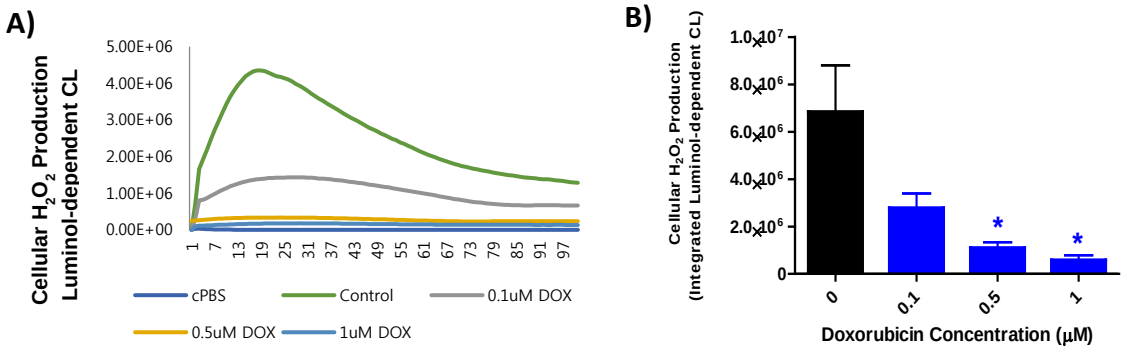

Figure 7. Effect of Dox Exposure on Intracellular H_2O_2 Levels in H9c2 Cells.

H9c2 cells (1 X 10^6) were suspended in complete PBS (cPBS) and incubated with different concentrations of Dox in presence of 10 μM luminol and 10 μg/ml horse radish peroxidase as described in "Materials and Methods," and chemiluminescence was recorded immediately. (A) Real-time measurement of the CL responses from the samples. (B) Area under the curve for each of the luminol-dependent CL response curves from the samples. *Data are mean ±SEM from three experiments. *P<0.05 compared to control group (n=3).*

Cellular Production of Hydrogen Peroxide in H9c2 Cells Following Exposure to Dox

Numerous studies have previously exhibited the role of ROS and oxidative stress in Dox-induced cardiotoxicity [58-60]. To investigate if exposures to low concentrations of Dox can still trigger cell-mediated redox cycling of Dox and stimulate ROS production

in H9c2 cells, luminol- and lucigenin-derived chemiluminescence (CL) assays were conducted. CL techniques have been commonly used to detect ROS production in both whole cells and isolated mitochondria [61-64]. In this study, luminol, in the presence of horseradish peroxidase (HRP), was used to detect H_2O_2 formation while lucigenin was used to detect superoxide in H9c2 cells. With regards to H_2O_2 presence, real-time CL data can be seen in figure 7. Luminol-derived CL was observed with H9c2 cells alone indicating the basal cellular level of H_2O_2 that plays a key role in cell survival and cell cycle. Interestingly, exposure to Dox resulted in decreased CL responses in a concentration-dependent manner, suggesting a reduction in r H_2O_2 presence. Significant H_2O_2 reduction was detected in cells treated with 0.5 and 1 µM of Dox ($p < 0.05$).

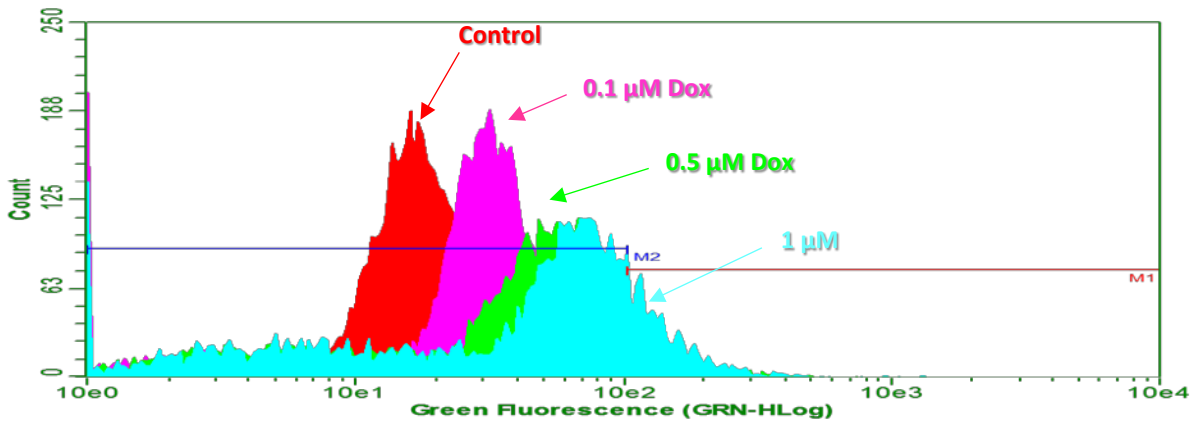

Figure 8. Flow Cytometric Analysis of Cellular H_2O_2 Presence in H9c2 Cells After Exposure to Dox.

H9c2 cells were exposed to various concentrations of Dox for 16 hours. Samples from the cell suspensions were initially analyzed with a microcapillary flow cytometry system (easyCyte, MilliporeSigma, USA) without any application of the fluorescence markers to the samples. Excitation wavelength of 488 nm was used, and the histogram was produced from the initial fluorescence observation using an emission filter with wavelength bandwidth capability of 525/30 nm. Data collected were analyzed in guavaSoft analysis software (MilliporeSigma, USA). Although no dyes were used, flow cytometric analysis shows significant shift across DCF-DA (Green Fluorescence) intensity by Dox treatment.

To further confirm our luminol-derived CL data, we conducted flow cytometric analysis on intracellular presence of hydrogen peroxide following exposures to low concentrations of Dox. DCF-DA, a fluorescent dye commonly used as indicators of hydrogen peroxide presence, was chosen because its excitation/emission spectra of 493/522 nm were in accord with the technical specifications of the esayCyte 5 flow cytometer used in the analysis. However, as shown in figure 8, a histogram representation of the initial analysis of the samples without the fluorescent marker DCF-DA showed a concentration-dependent shift that was almost a log order greater than the control group. This result accentuated the significance of the partial overlap in fluorescence spectra of DCF-DA and Dox (Refer to Fig. 5-B) while providing evidence that the innate fluorescence of Dox can interfere with the DCF-DA flow cytometry assay.

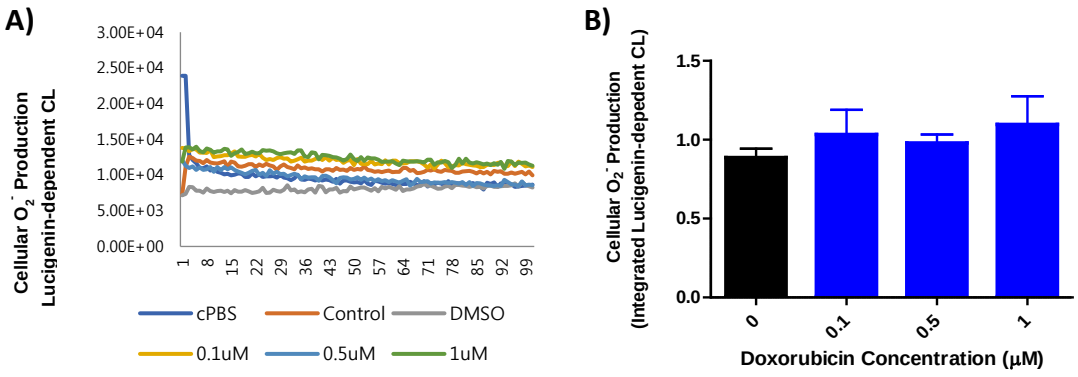

Figure 9. Effect of Dox Exposure on Intracellular Superoxide Levels in H9c2 Cells.

H9c2 cells (1 X 10^6) were suspended in air-saturated complete phosphate buffered saline (cPBS) and incubated with different concentrations of Dox in presence of 10 µM lucigenin as described in the "Materials and Methods," and chemiluminescence was recorded immediately. (A) Real-time measurement of the lucigenin-derived CL responses from the samples. X-axis represents time points (30 minutes divided into 100 time points). Y-axis represents fluorescence events. (B) Area under the curve for each of the CL response curves from the samples. *Data for panel B represent mean ±SEM. *P<0.05 compared to control group (n=3).*

In addition, lucigenin-derived CL detection assay was implemented to detect superoxide presence in H9c2 cells following exposures to low concentrations of Dox. Lucigenin-derived CL responses were not observed following Dox treatment suggesting that Dox, at concentrations below 1 μM, does not induce significant superoxide production in H9c2 cells (Fig. 9).

Decrease in Mitochondrial Hydrogen Peroxide Presence Following Exposure to Dox

Previous studies suggested that the mitochondria may be critically involved in mediating the redox cycling of Dox to produce ROS in cardiomyocytes [42, 65-67]. To further examine the effect of Dox on mitochondrial hydrogen peroxide presence and the subsequent role it may have in Dox-induced cytotoxicity, mitochondria were isolated from the H9c2 cells. 9,10-Phenanthraquinone (PNQ), a compound previously identified to undergo redox cycling to produce ROS [68], was implemented as a positive control to induce ROS production (Fig. 10A).

As shown in Fig. 10 B-C, incubation of succinate-supplemented mitochondria in various concentrations of Dox (0.1, 0.5, 1 μM) resulted in a concentration-dependent decrease in luminol-derived CL, indicating a reduction in mitochondrial hydrogen peroxide presence, corresponding to the observation of cellular hydrogen peroxide in intact H9c2 cells following exposure to the same concentrations of Dox (Fig. 7). Also, addition of Dox to substrate-supported mitochondria did not have any significant effect on lucigenin-derived CL (Fig. 11), suggesting that low concentrations of Dox does not trigger the production of mitochondria-derived superoxide in H9c2 cells.

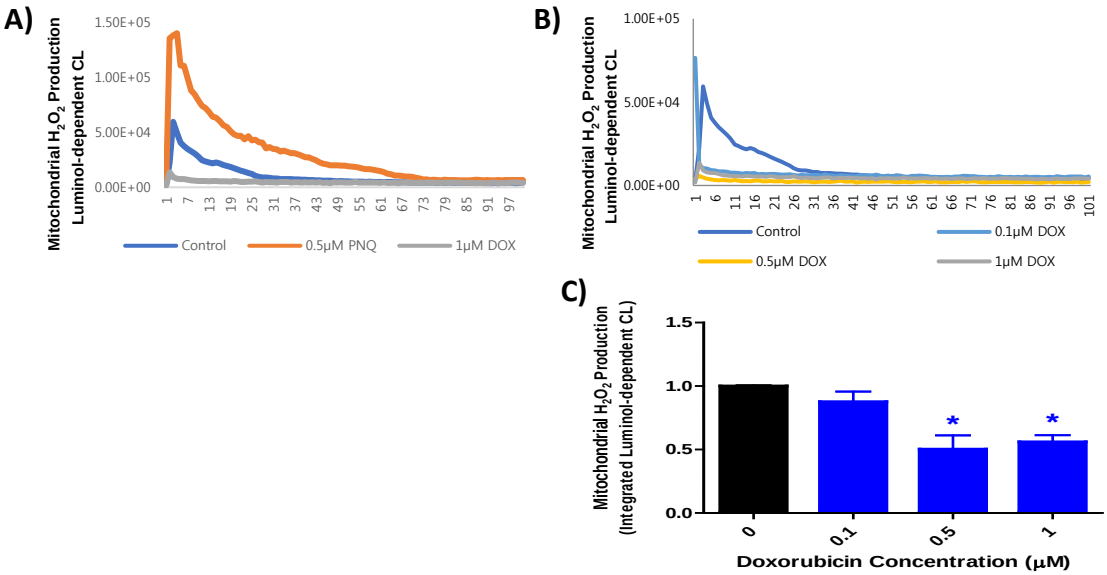

Figure 10. Effect of Dox Exposure on Mitochondrial H_2O_2 Levels.

Mitochondrial hydrogen peroxide was detected by luminol-derived chemiluminescence in the mitochondrial extract of H9c2 cells. Mitochondria were isolated from freshly harvested H9c2 cells. 25 µg/ml of mitochondrial extract was incubated with varying concentration of Dox or PNQ in presence of succinate. (A) Comparison of real-time CL responses from the control group and the experimental groups exposed to either 0.5 µM PNQ or 1 µM Dox. (B) Comparison of real-time CL responses from the control group and the experimental groups exposed to either 0.1, 0.5, or 1 µM Dox. (C) Area under the curve representation for each of the CL response curves from panel B. *Data for panel C represent mean ±SEM. *P<0.05 compared to control group (n=3).*

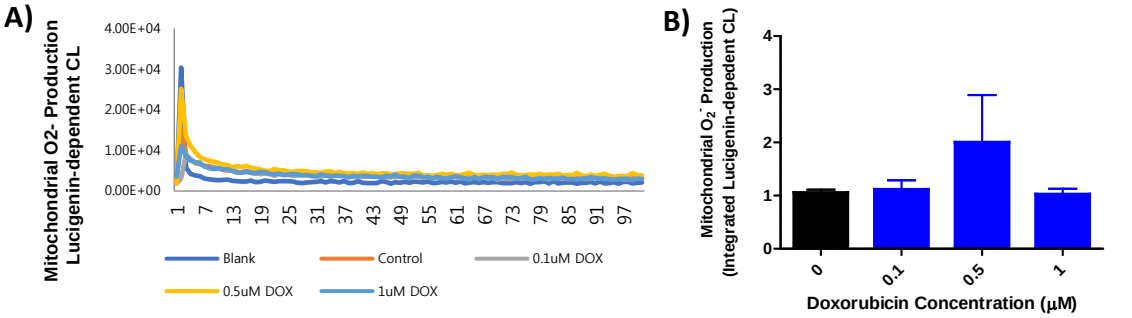

Figure 11. Lucigenin-Derived Chemiluminescence Responses Indicate No Significant Change in Superoxide in Mitochondria of H9c2 Cells Following Dox Treatment.

Mitochondrial superoxide was detected by lucigenin-derived chemiluminescence in the mitochondrial extract of H9c2 cells. Mitochondria were isolated from freshly harvested H9c2 cells. 50 µg/ml of mitochondrial extract was incubated with varying concentration of Dox. (A) Real-time measurement of the CL responses from the samples. (B) Area under the curve for each of the CL response curves from the samples. *Data represent mean ± SEM. *P<0.05 compared to control group (n=3).*

Effects of Dox on Components of Cellular Antioxidative Response in H9c2 Cells

Glutathione (GSH) is one of the most vital components of cellular antioxidative responses against exogenously or endogenously produced reactive oxygen and nitrogen species (ROS and RNS). To investigate the effects of low concentrations of Dox on intracellular levels of GSH, H9c2 cells were exposed to various concentrations of Dox for 24 hours. The effect of Dox on GSH content was examined using an OPT-GSH fluorescence assay. As depicted in figure 11-A, there was a significant increase in cellular GSH level after exposure to 0.5 µM Dox. However, treatment with 1 µM Dox did not show any significant change in cellular GSH content level compared to the control group. Another important component in cells efforts to maintain redox balance is the activity of phase II detoxification enzymes. Enzymatic activities of both NQO1 and GST, key phase II enzymes, were determined by quantitatively measuring the rate of NADPH oxidation.

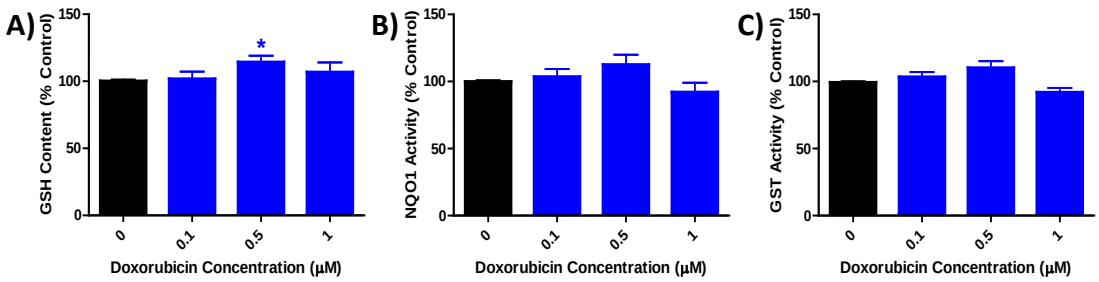

Figure 12. Effect of Dox Treatment on GSH Content and Enzymatic Activities of NQO1 and GST in Cells Treated With or Without Various Concentrations of Dox.

H9c2 cells were incubated with indicated concentrations of Dox for 24 hours. Cells were collected and processed for measurement of total cellular GSH content (A), NQO1 activity (B), and GST activity (C). *All data represent mean ± SEM. *P<0.05 in comparison to the control group (n=4).*

As depicted in figure 12, the activities of cellular NQO1 and GST did not deviate much from those of the control groups, although the activity rates for both enzymes displayed an increasing trend up to the 0.5 µM Dox treatment. qRT-PCR analysis was performed to evaluate the effects of Dox treatment on gene expression levels of *GCLC* and *NOQ1*. *GCLC* encodes for the catalytic subunit of glutamate-cysteine ligase, a key enzyme in the synthesis of GSH. H9c2 cells showed significant increases in the expression of *GCLC* and *NQO1* following 16 hours of 0.5 µM Dox treatment (Fig. 13).

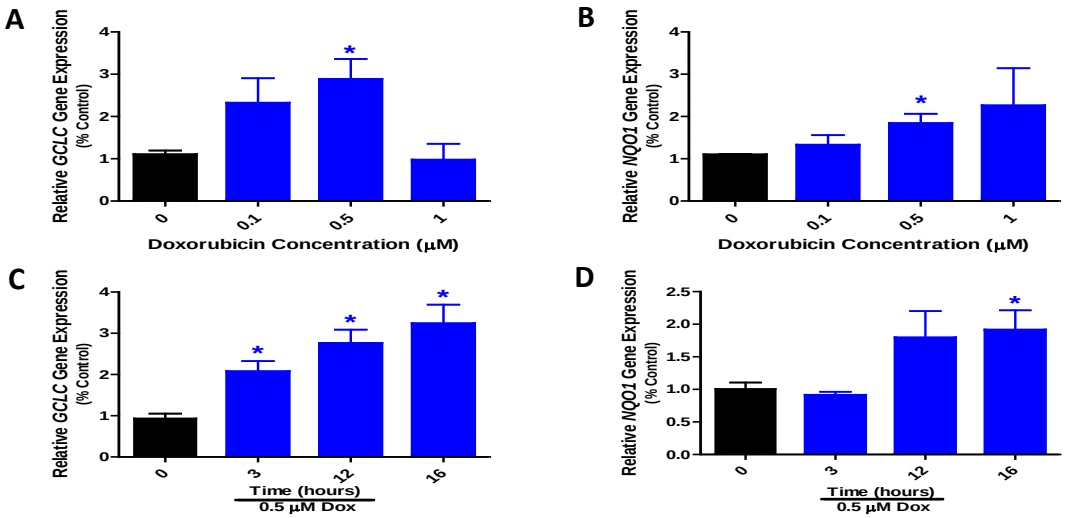

Figure 13. Dox Treatment Up-Regulates the Gene Expressions of *GCLC* and *NOQ1* in H9c2 Cells.

H9c2 cells were exposed to indicated concentrations of Dox for 16 hours (A and B) or to 0.5 µM Dox for various hours (C and D). The relative mRNA abundance in each sample was evaluated by real-time PCR and changes in transcript abundance were normalized based on the mean of control gene GAPDH. *All data represent mean ± SEM. *P<0.05 in comparison to the control group (n=3).*

Overall, the gene expressions of both *GCLC* and *NQO1* produced similar dose-dependent trends to which were also observed in cellular GSH content and NQO1 enzymatic activity levels (Fig. 12). Figure 13-C shows time-dependent observations of

GCLC expression with a significant increase in *GCLC* expression beginning with 3 hours of exposure to 0.5 µM Dox. Similar time-dependent observation of *NQO1* gene expression showed nearly a two-fold increase after 12 hours and a significant increase in *NQO1* expression after 16 hours of exposure to 0.5 µM Dox (Fig. 13-D).

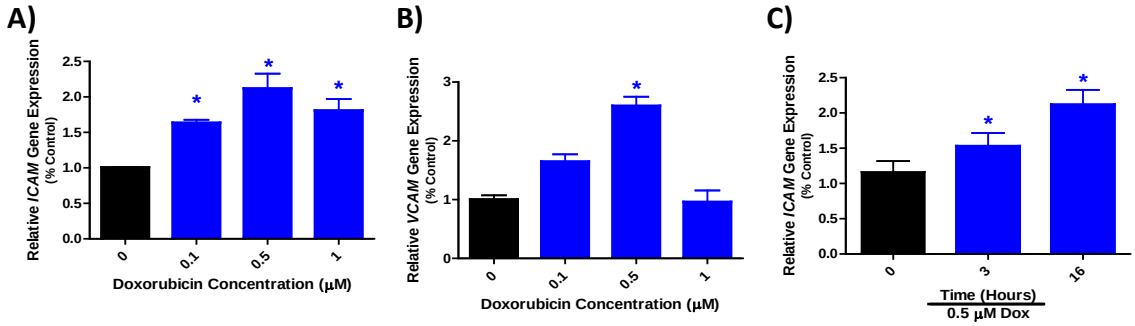

Figure 14. Dox Treatment Up-Regulates the Gene Expressions of Proinflammatory Genes *ICAM* and *VCAM* in H9c2 Cells.

H9c2 cells were exposed to indicated concentrations of Dox for 16 hours (A and B) or to 0.5 µM Dox for various hours (C and D). The relative mRNA abundance in each sample was evaluated by real-time PCR and changes in transcript abundance were normalized based on the mean of control gene GAPDH. *All data represent mean ± SEM. *P<0.05 in comparison to the control group (n=3).*

Upregulation of Inflammatory Response Genes

Expressions of various inflammatory mediators such as intracellular adhesion molecule-1 (ICAM-1), and vascular cell adhesion molecule-1 (VCAM-1) have been implicated in doxorubicin- induced cardiotoxicity [37]. In the same experiments described for the gene expression of GCLC an NQO1 (Figure 13), the effects of Dox on the expression levels for inflammatory marker genes *ICAM* and *VCAM* were determined via qRT-PCR. Figure 14-A illustrates a dose-dependent increase in *ICAM* expression following treatments of 0, 0.1, 0.5, and 1uM Dox for 16 hours. Panel B describes similar

dose-dependent increase in *VCAM* expression up to 0.5 µM followed by decrease in the gene expression level that was comparable to that of the control group. Time-dependent observations of *ICAM* expression supported the dose-dependent observation as significant increase in *ICAM* expression was observed after 3 hours of exposure to 0.5 µM Dox.

Upregulation of GSH and NQO1 by CDDO-Im Provided Minimal Protection Against Dox-induced Cytotoxicity

To further investigate the role of oxidative stress on Dox-induced cytotoxicity, antioxidant response of H9c2 upon exposure to Dox was augmented by CDDO-Im. CDDO-Im is a synthetic triterpenoid previously characterized as being potent in providing protection against several types of oxidative stress [69].

Panels A and B of figure 15 represent significant increases in gene expressions of both *NQO1* and *GCLC* following 3-hour and 6-hour exposure to 100 nM of CDDO-Im. Panels C and D of the same figure depicts quantitative calculation of cellular GSH presence and NQO1 activity following a 24-hour exposure to 100 nM of CDDO-Im. To study whether upregulated levels of GSH and NQO1 by CDDO-Im can protect cells against Dox-induced cytotoxicity, we co-treated 100nM of CDDO-Im with various concentrations of Dox for 24 hours. As shown in figure 14-E, incubation of H9c2 cells with various concentrations of Dox for 24 h led to significant decreases in cell viability, as detected by MTT reduction assay. Co-treatment of cells with 100 nM CDDO-Im afforded a significant protection against cytotoxicity induced by Dox at 0.5 µM.

However, treatments involving greater than 1 µM of Dox showed no cytoprotection (Fig. 15-E).

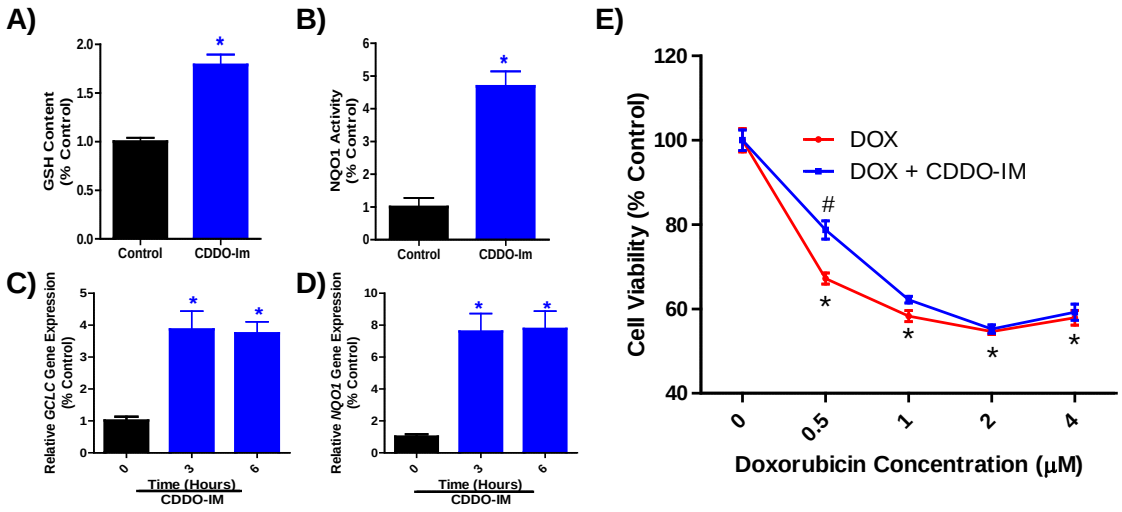

Figure 15. Upregulation of GSH and NQO1 by CDDO-Im Provided Minimal Protection Against Dox-induced Cytotoxicity in H9c2 Cells.

H9c2 cells were treated with either vehicle DMSO or 100uM CDDO-Im in DMSO for 6 hours (A& B) or up to 6 hours (C& D). Panels A and B indicated total cellular GSH content and NQO1 enzymatic activity, respectively, following a 6-hour treatment with 100nM CDDO-Im. Panels C and D indicate qualitative analysis of NQO1 and GCLC mRNA expression, respectively, at the indicated time points after treatment with 100nM CDDO-Im for 0, 3, and 6 hours. Both values were relative to those of each control group. *All data represent mean ± SEM. *P<0.05 in comparison to the control group (n=3).* In Panel E, the cells were co-treated with 100nM of CDDO-Im and various concentrations of Dox for 24 hours. Cell viability was then measured using MTT assay. *All data represent mean ±SEM. *, p<0.05 vs. control; #, p<0.05 vs. Dox alone-treated cells (n=8).*

CHAPTER IV

DISCUSSION

Doxorubicin's prominence as one of the most successful chemotherapeutic agents treating a wide range of cancers has endured for over 40 years. Although Dox remains one of the most effective antineoplastic agents, Dox-induced cardiotoxicity leading to heart failure has been recognized as a frequent problem and hallmark side effect related to cumulative dose of Dox administered over the lifetime of the recipient. Many of previous studies demonstrated that Dox may exert the cardiotoxicity by increases in oxidative stress [14, 17], DNA damage leading to impeded synthesis of biomolecules, decrease in the expression of antioxidants [17, 18], and mitochondrial dysfunction [19]. However, the concentrations of Dox used in most of these studies are not physiologically relevant in some cases, the treatment concentrations are several log orders higher than the clinically-observed concentrations [46-55].

Of course, due to the complexity and variability of the immediate interaction between Dox and the physiological environment of the system into which it has been injected, it is nearly impossible to precisely define "clinically-relevant concentration of Dox" with an exact value. It is only possible to deduce a range of values based on data from various clinical studies. Several studies in their attempts to provide the necessary data have shown that clinically-observed concentrations of Dox vary mostly on the method of administration. For bolus administration of Dox, initial plasma concentration,

in general, was observed to be between 1 to 2 uM [57, 70, 71] while continuous infusion administration of Dox showed initial plasma concentration of Dox falling into the range of 25-250 nM [72]. Therefore, in order for the results of this study to more accurately reflect the mechanism of doxorubicin-induced cardiotoxicity, the current study involving the H9c2 rat cardiomyocyte was designed to utilize various concentrations of Dox less than 2uM. As our experimental model system, H9c2 rat cardiomyoblasts were used in current investigation because these clonal cardioblasts from the rat heart are used extensively in *in vitro* model for studies associated with cardiomyocyte physiology including ischemia, reperfusion injury, and chronic heart failure [73-75].

To first examine the cytotoxic effect of Dox at clinically-relevant concentrations, we used 3-(4, 5-dimethylthiazolyl-2)-2, 5-diphenyltetrazolium bromide (MTT) cell viability assay, one of the most widely-used cell viability assays that is dependent on the cells' metabolic capability to reduce MTT into formazan crystals. Through this analysis, we demonstrated that the cell viability decreased following a 24-hour of treatment with both 0.5 and 1 μM Dox. Time-dependent observation of the same analysis revealed that the cytotoxic effect of 0.5 and 1 μM Dox on H9c2 cells begins after 12 hours (Figs. 2 & 3). We then tried to confirm our data from the MTT cell viability analysis by quantitatively measuring LDH release. LDH is a cytosolic enzyme and can be leaked out from cells when the plasma membranes are damaged. Therefore, the release of the LDH is a key signature for necrotic cell death due to plasma membrane damage. However, the quantitative analysis of LDH release suggested a significant LDH release following a 24-hour exposure to 2 μM Dox, indicating Dox-induced necrosis death only at 2 μM (Fig. 3-

B). Considering that MTT-reduction assay measures mitochondrial respiration activity rate as an indicator of cell viability while LDH release is a good indicator for necrosis, we tentatively interpreted the discrepancy from the two viability assays as evidence that may suggest that exposure to low concentrations of Dox (up to 1 μM) mainly compromised mitochondrial function while exposure to high concentrations of Dox can cause necrosis in H9c2 cells. In a temporal perspective, it provides evidence that compromised mitochondrial function precedes the impediment of cellular membrane integrity.

In our efforts to further investigate the extent to which both apoptotic and necrotic modes of cell death characterize Dox-induced cell death at various concentrations, we conducted fluorescence-based Annexin V FITC/PI flow cytometric cell viability assay. However, the data from the flow cytometric analysis showed a significant increase in FITC-positive cells from Dox treatment group even when no FITC fluorescent marker was applied to the cells (Fig. 4). This suggested that the intensity of the innate fluorescence of Dox may be potent enough to be detected by flow cytometer, producing results that may lead to misrepresentation of the proportion of apoptotic cells. To elucidate the possible interference effect of Dox fluorescence on the Annexin V FITC/PI cell viability assay, fluorometric analysis of Dox was done to characterize the its innate fluorescence property.

As shown in figure 5-A, Dox was found to exhibit fluorescence spectra consisting of a maximum excitation wavelength of 493 nm and a maximum emission wavelength of 592 nm. When the fluorescence spectra of Dox was compared to the

fluorescent spectra of multiple fluorescent probes and markers used to assess cell viability and ROS presence, it was found that fluorescent indicators, DCF-DA, FITC, MitoSOX, and PI, utilized in these assays exhibited fluorescence spectrometric characteristics that were, in varying degrees, similar to that of Dox (Fig 5-B). It is important to note that FITC conjugated Annexin V has been widely used *in the past three decades* to determine prevalence of apoptosis in Dox-induced cell death in various cells and tissues [76-82]. However, these studies failed to mention innate fluorescence capability of Dox and how such property may produce misleading results. Our data suggest that such inherent fluorescence capability of Dox be considered when investigative procedures require the use of fluorescence-based assays such as the MitoSOX- or the DCFDA-integrated ROS detection assays or the Annexin V FITC/PI-integrated cell death determination assay.

The intrinsic fluorescence of Dox allowed Dox, at clinically-relevant concentrations, to be detectable at cellular level not only by flow cytometry, but also by spectrofluorometric measurement and fluorescence microscopic imaging as shown in figure 5. Incubation of H9c2 cells with Dox resulted in time-dependent intracellular amassing of Dox (Fig. 6B). The fluorescence microscopic imaging of H9c2 cells having been exposed to Dox confirmed the spectrofluorometric measurement on intracellular accumulation of Dox and, even more, revealed that the intracellular accumulation of Dox was more prevalent in the nuclear region than the cytoplasm of the cells (Fig 6C). The cellular uptake assay used in the current study may be of importance towards validating

the practicality of utilizing the fluorescence capability of Dox as a tool for future investigations of Dox-induced cytotoxicity. Such confirmation will certainly lead to the development of novel methods that may further elucidate the details of Dox uptake and distribution which will clarify the interaction between Dox and various intracellular components instrumental in Dox-induced cardiotoxicity.

Previous studies have indicated redox cycling of quinone moiety of Dox resulting in overproduction of ROS that eventually overcome cells' natural detoxification measures leading to the subsequent oxidative stress as the primary event responsible for Dox-induced cardiotoxicity. It is suggested that the quinone moiety of doxorubicin can accept an electron to produce the semiquinone form of doxorubicin. Incomplete reduction of molecular oxygen can cause the redox cycling of doxorubicin as the semiquinone form is oxidized back to the original quinone form. During this process, the molecular oxygen becomes incompletely reduced into a superoxide anion radical ($O_2^{\bullet -}$) [23]. However, based on the results from the current study, we do not believe that the overproduction of ROS and its association with the oxidative stress are primary driving forces behind Dox-induced cardiotoxicity following exposure to clinically-relevant concentrations of Dox. Firstly, as stated earlier, most of the studies reporting ROS production involved Dox concentrations that were well above those observed in clinical settings. Secondly, some of the evidence advocating ROS production was derived from fluorescence-based investigations, such as DCF-DA-integrated ROS detection [83-87], that failed to consider the inherent fluorescence of Dox. These authors failed to distinguish whether the increase

in fluorescence intensity was due to increase in ROS production or simply due to increased cellular accumulation of Dox. Thirdly, our data suggests that Dox, at clinically relevant concentrations, significantly decreased hydrogen peroxide presence in H9c2 cells in an inverse concentration-dependent manner (Fig.7). Fourthly, upregulation of GSH and NQO1 by CDDO-Im provided only minimal protection against Dox-induced cytotoxicity in H9c2 cells (Fig. 15). Lastly, consistent to our *in vitro* results, many of the previous studies have suggested that ROS scavengers failed to prevent cardiotoxicity [58-60] while some studies failed to detect free radicals even at supraclinical Dox concentrations [88-90].

Mammalian cells have evolved an efficient ROS detoxifying system to protect cells from oxidative damage. ROS detoxification system included GSH and NQO1 and others [91-93]. In this study, exposure to Dox at clinically relevant concentrations led to significant increase in the expressions of GSH and NQO1 genes in a dose- and time-dependent manner (Figs. 13). Induction of GHS and NQO1 by Dox may diminish the endogenous basal hydrogen peroxide, which functions as a component of redox homeostasis as well as an intracellular signal. Thus, it is likely that Dox can stimulate an intracellular anti-oxidative response that can blunt normal ROS signaling when there is an imbalance between the ROS detoxification system and the endogenous basal ROS production, which further leads to induce inflammation in cardiomyocytes by increases in gene expression of adhesion molecules like *VCAM-1* and *ICAM-1* (Fig. 14). The0 expression of adhesion molecules and cytokines was found to exhibit a role in the multi-

factorial cardiomyopathy induced by Dox [32, 37]. However, how Dox stimulates ROS detoxifying antioxidants/enzymes like GSH and NQO1 remains unclear. Studies showed that activation of nuclear factor-erythroid 2-related factor 2 (Nrf2) has been reported to coordinately upregulate GSH and NQO1 as well as other ROS detoxification enzymes both in *in vitro and in vivo* [94-98].

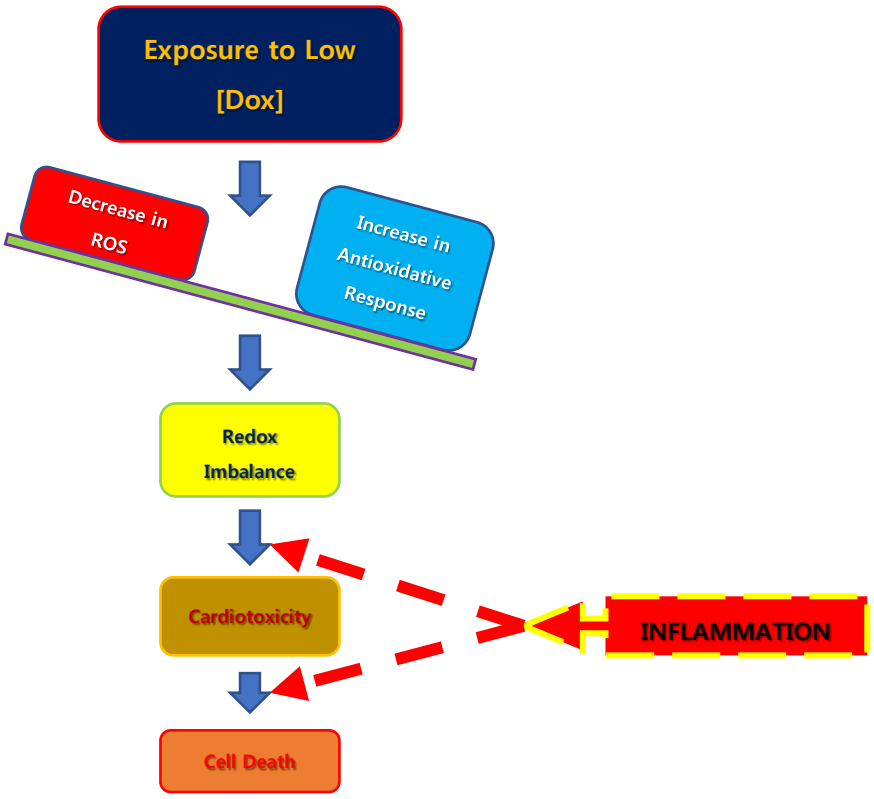

Figure 16. Dox-Induced Cardiotoxicity on H9c2 Cells Following Exposure to Physiologically Relevant Concentrations of Dox.

Diagram of prosed roles ROS and redox balance on the development of Dox-induced cardiotoxicity in H9c2 rat cardiomyoblasts. Increased anti-oxidative response and decreased ROS presence results in redox imbalance. One of the ways that this can be detrimental to the cells is that such redox imbalance can compromise ROS-dependent cell signaling pathways that are often associated with cell survival and proliferation. Increased expression of pro-inflammatory genes provide evidence that inflammation takes part in the process. However, it is unsure if inflammation is a contributing cause towards cardiotoxicity or a consequence result from cardiotoxicity and is playing a role in cell death.

Nrf2 is a critical transcription factor that binds to the antioxidant response element (ARE) in the promoter region of multiple genes whose products regulate an array of cellular activities related to cell proliferation, defense, and signal transduction [94-98]. A significant decrease in the expression and induction of NQO1 in *Nrf2*-disrupted mice further confirmed the role of Nrf2 in ARE-mediated antioxidant response [99]. The Nrf2-dependent anti-oxidative pathway is seemingly the most important in terms of host cell's defense against stress from excess ROS and electrophiles due to introduction of exogenous and endogenous chemicals, metals, and radiation [100]. In response to various stimuli, Nrf2 is released from Keap-1 and translocated into the nucleus to form heterodimers with Maf proteins. This complex bind to antioxidant response element (ARE) of the promoter region of antioxidant genes stimulating their expression [101]. Examination of the direct effect of Dox on the Nrf2/ARE signaling pathway will contribute to understanding the action of Dox in stimulating GSH and NOQ1. Activation of Nrf2/ARE pathway would dampens the redox homeostasis that may be involved in Dox-induced cardiotoxicity.

Previous studies showed that mitochondria play a crucial role in generation of substantial amounts of ROS by electron leakage from the oxidative phosphorylation pathway and mitochondrial electron transport chain (METC) has been shown to be one of the main locations redox cycling of Dox to generate ROS [14, 19]. One of the unique characteristics of cardiomyocytes is the increased oxidative metabolism due to the abundance of mitochondria. In this study, with mitochondria isolated from H9c2 cells, Dox at clinically relevant plasma concentrations also led to decreases in basal hydrogen

peroxide (Fig. 10), the similar effects observed with intact cells (Fig. 7). Thus, the results with isolated intact mitochondria demonstrated that Dox could particularly target mitochondria and subsequently decrease basal ROS production. Lucigenin-derived CL was further employed to detect mitochondria-derived superoxide production. However, addition of Dox to succinate-supported mitochondria has no effect on lucigenin-derived CL. A previous study showed that lucigenin-derived CL is highly dependent on the mitochondrial membrane potential [62]. Thus, the failure of Dox to effect on the lucigenin-derived CL both in intact H9c2 cells and the isolated mitochondria (Figs. 9 and 11) can occur when Dox damages the mitochondrial membrane potential. Mitochondrial complexes have been shown to be involved in the reduction of molecular oxygen to superoxide and mitochondrial complex I has been suggested to be the specific site in catalyzing the redox cycling of Dox [14, 19]. Also, Dox has been found to have high affinity for mitochondrial DNA. Studies involving bolus and continuous infusion administrations of Dox showed accumulation of 8-hydroxydeoxyguanosine, a biomarker for DNA damage, preferentially in mitochondrial DNA when compared with nuclear DNA [102, 103]. Since *TOPO2B* is also expressed in the mitochondrial DNA, Dox inhibition of topoisomerase IIβ in the mtDNA may result in mitochondrial dysfunction and cause electron leakage along with superoxide formation from the METC. Future work could investigate how Dox at varying clinically relevant plasma concentrations affect the mtDNA damage and the role of cytochrome c release from mitochondria into the soluble cytoplasm in triggering Dox-induced cell death.

In summary, this study demonstrates that exposure to Dox at clinically relevant plasma concentrations (0.1-2μM) significantly decreased hydrogen peroxide levels in an inverse concentration-dependent manner both in intact H9c2 rat cardiomyocyte H9c2 cells and the isolated mitochondria. H9c2 cells treated with Dox showed a significant increase in the expressions of genes for intracellular anti-oxidative response that can blunt normal ROS signaling and thus may induce inflammation in cardiomyocytes. This study may contribute to the understanding of mechanism associated with increased risk of cardiotoxicity by Dox, which is an important component of various chemotherapy regimens.

REFERENCES

1. Hilmer, S.N., et al., *The hepatic pharmacokinetics of doxorubicin and liposomal doxorubicin.* Drug Metab Dispos, 2004. **32**(8): p. 794-9.

2. Smith, L.A., et al., *Cardiotoxicity of anthracycline agents for the treatment of cancer: systematic review and meta-analysis of randomised controlled trials.* BMC Cancer, 2010. **10**: p. 337.

3. Chatterjee, K., et al., *Doxorubicin cardiomyopathy.* Cardiology, 2010. **115**(2): p. 155-162.

4. Levine, A.J., *p53, the Cellular Gatekeeper for Growth and Division.* Cell, 1997. **88**(3): p. 323-331.

5. Perego, P., et al., *Role of apoptosis and apoptosis-related genes in cellular response and antitumor efficacy of anthracyclines.* Curr Med Chem, 2001. **8**(1): p. 31-7.

6. Dimarco, A., et al., *[Research on the Activity of Daunomycin on Normal and Neoplastic Cells Cultivated in Vitro]*. Tumori, 1963. **49**: p. 235-51.

7. Dalmark, M., *Characteristics of doxorubicin transport in human red blood cells.* Scand J Clin Lab Invest, 1981. **41**(7): p. 633-9.

8. Tacar, O., P. Sriamornsak, and C.R. Dass, *Doxorubicin: an update on anticancer molecular action, toxicity and novel drug delivery systems.* J Pharm Pharmacol, 2013. **65**(2): p. 157-70.

9. Booth, C.L., K.R. Brouwer, and K.L. Brouwer, *Effect of multidrug resistance modulators on the hepatobiliary disposition of doxorubicin in the isolated perfused rat liver.* Cancer Res, 1998. **58**(16): p. 3641-8.

10. Lipp, H.-P., *Anticancer drug toxicity : prevention, management, and clinical pharmacokinetics.* 1999.

11. Buzdar, A.U., et al., *Early and delayed clinical cardiotoxicity of doxorubicin.* Cancer, 1985. **55**(12): p. 2761-2765.

12. Von Hoff, D.D., et al., *Risk factors for doxorubicin-induced congestive heart failure.* Ann Intern Med, 1979. **91**(5): p. 710-7.

13. Swain, S.M., F.S. Whaley, and M.S. Ewer, *Congestive heart failure in patients treated with doxorubicin: a retrospective analysis of three trials.* Cancer, 2003. **97**(11): p. 2869-79.

14. Takemura, G. and H. Fujiwara, *Doxorubicin-induced cardiomyopathy from the cardiotoxic mechanisms to management.* Prog Cardiovasc Dis, 2007. **49**(5): p. 330-52.

15. Praga, C., et al., *Adriamycin cardiotoxicity: a survey of 1273 patients.* Cancer Treat Rep, 1979. **63**(5): p. 827-34.

16. Lefrak, E.A., et al., *A clinicopathologic analysis of adriamycin cardiotoxicity.* Cancer, 1973. **32**(2): p. 302-14.

17. Singal, P.K. and N. Iliskovic, *Doxorubicin-induced cardiomyopathy.* New England Journal of Medicine, 1998. **339**(13): p. 900-905.

18. Powell, S.R. and M. Chevion, *The effect of chronic administration of doxorubicin on the rat cardiac and hepatic glutathione redox system.* Res Commun Chem Pathol Pharmacol, 1991. **74**(3): p. 273-86.

19. Doroshow, J.H. and K.J. Davies, *Redox cycling of anthracyclines by cardiac mitochondria. II. Formation of superoxide anion, hydrogen peroxide, and hydroxyl radical.* J Biol Chem, 1986. **261**(7): p. 3068-74.

20. Keith, M., et al., *Increased oxidative stress in patients with congestive heart failure.* J Am Coll Cardiol, 1998. **31**(6): p. 1352-6.

21. Lee, V., A.K. Randhawa, and P.K. Singal, *Adriamycin-induced myocardial dysfunction in vitro is mediated by free radicals.* Am J Physiol, 1991. **261**(4 Pt 2): p. H989-95.

22. Singh, N., et al., *Oxidative stress and heart failure.* Mol Cell Biochem, 1995. **147**(1-2): p. 77-81.

23. D'Autreaux, B. and M.B. Toledano, *ROS as signalling molecules: mechanisms that generate specificity in ROS homeostasis.* Nat Rev Mol Cell Biol, 2007. **8**(10): p. 813-24.

24. Miller, D.M., G.R. Buettner, and S.D. Aust, *Transition metals as catalysts of "autoxidation" reactions.* Free Radic Biol Med, 1990. **8**(1): p. 95-108.

25. Li, Y.R., Z. Jia, and M.A. Trush, *Defining ROS in Biology and Medicine.* 2016, 2016. **1**(1): p. 13.

26. Noubade, R., et al., *NRROS negatively regulates reactive oxygen species during host defence and autoimmunity.* Nature, 2014. **509**(7499): p. 235-9.

27. Breimer, L.H., *Molecular mechanisms of oxygen radical carcinogenesis and mutagenesis: the role of DNA base damage.* Mol Carcinog, 1990. **3**(4): p. 188-97.

28. Lakshmi, S.V., et al., *Oxidative stress in cardiovascular disease.* Indian J Biochem Biophys, 2009. **46**(6): p. 421-40.

29. Last, J.A., W.M. Sun, and H. Witschi, *Ozone, NO, and NO2: oxidant air pollutants and more.* Environ Health Perspect, 1994. **102 Suppl 10**: p. 179-84.

30. Meneghini, R., *Iron homeostasis, oxidative stress, and DNA damage.* Free Radic Biol Med, 1997. **23**(5): p. 783-92.

31. Los, M., et al., *Hydrogen peroxide as a potent activator of T lymphocyte functions.* Eur J Immunol, 1995. **25**(1): p. 159-65.

32. Valko, M., et al., *Free radicals and antioxidants in normal physiological functions and human disease.* Int J Biochem Cell Biol, 2007. **39**(1): p. 44-84.

33. Baud, V. and M. Karin, *Signal transduction by tumor necrosis factor and its relatives.* Trends Cell Biol, 2001. **11**(9): p. 372-7.

34. Zoico, E., et al., *The effects of adiponectin on interleukin-6 and MCP-1 secretion in lipopolysaccharide-treated 3T3-L1 adipocytes: role of the NF-kappaB pathway.* Int J Mol Med, 2009. **24**(6): p. 847-51.

35. Kim, S.R., et al., *Visfatin enhances ICAM-1 and VCAM-1 expression through ROS-dependent NF-kappaB activation in endothelial cells.* Biochim Biophys Acta, 2008. **1783**(5): p. 886-95.

36. Lee, W.J., et al., *Visfatin-induced expression of inflammatory mediators in human endothelial cells through the NF-kappaB pathway.* Int J Obes (Lond), 2009. **33**(4): p. 465-72.

37. Ehrke, M.J., et al., *Correlation between adriamycin-induced augmentation of interleukin 2 production and of cell-mediated cytotoxicity in mice.* Cancer Res, 1986. **46**(1): p. 54-60.

38. Droge, W., *Free radicals in the physiological control of cell function.* Physiol Rev, 2002. **82**(1): p. 47-95.

39. Burhans, W.C. and N.H. Heintz, *The cell cycle is a redox cycle: linking phase-specific targets to cell fate.* Free Radic Biol Med, 2009. **47**(9): p. 1282-93.

40. Babior, B.M., R.S. Kipnes, and J.T. Curnutte, *Biological defense mechanisms. The production by leukocytes of superoxide, a potential bactericidal agent.* J Clin Invest, 1973. **52**(3): p. 741-4.

41. Piquereau, J., et al., *Mitochondrial dynamics in the adult cardiomyocytes: which roles for a highly specialized cell?* Front Physiol, 2013. **4**: p. 102.

42. Nicolay, K., et al., *The interaction of adriamycin with cardiolipin in model and rat liver mitochondrial membranes.* Biochim Biophys Acta, 1984. **778**(2): p. 359-71.

43. Doroshow, J.H., G.Y. Locker, and C.E. Myers, *Enzymatic defenses of the mouse heart against reactive oxygen metabolites: alterations produced by doxorubicin.* J Clin Invest, 1980. **65**(1): p. 128-35.

44. Rhee, S.G., et al., *Controlled elimination of intracellular H(2)O(2): regulation of peroxiredoxin, catalase, and glutathione peroxidase via post-translational modification.* Antioxid Redox Signal, 2005. **7**(5-6): p. 619-26

45. Sies, H., *Oxidative stress: oxidants and antioxidants.* Exp Physiol, 1997. **82**(2): p. 291-5.

46. Bachur, N.R., S.L. Gordon, and M.V. Gee, *Anthracycline antibiotic augmentation of microsomal electron transport and free radical formation.* Mol Pharmacol, 1977. **13**(5): p. 901-10.

47. Bates, D.A. and C.C. Winterbourn, *Deoxyribose breakdown by the adriamycin semiquinone and H2O2: evidence for hydroxyl radical participation.* FEBS Lett, 1982. **145**(1): p. 137-42.

48. Benchekroun, M.N., B.K. Sinha, and J. Robert, *Doxorubicin-induced oxygen free radical formation in sensitive and doxorubicin-resistant variants of rat glioblastoma cell lines [corrected and republished erratum originally printed in FEBS Lett 1993 May 17;322(3):295-8]*. FEBS Lett, 1993. **326**(1-3): p. 302-5.

49. Eliot, H., L. Gianni, and C. Myers, *Oxidative destruction of DNA by the adriamycin-iron complex.* Biochemistry, 1984. **23**(5): p. 928-36.

50. Feinstein, E., E. Canaani, and L.M. Weiner, *Dependence of nucleic acid degradation on in situ free-radical production by adriamycin.* Biochemistry, 1993. **32**(48): p. 13156-61.

51. Graham, M.A., et al., *The effect of the anthrapyrazole antitumour agent CI941 on rat liver microsome and cytochrome P-450 reductase mediated free radical processes. Inhibition of doxorubicin activation in vitro.* Biochem Pharmacol, 1987. **36**(20): p. 3345-51.

52. Lown, J.W., et al., *Strand scission of DNA by bound adriamycin and daunorubicin in the presence of reducing agents.* Biochem Biophys Res Commun, 1977. **76**(3): p. 705-10.

53. Muindi, J.R., et al., *Hydroxyl radical production and DNA damage induced by anthracycline-iron complex.* FEBS Lett, 1984. **172**(2): p. 226-30.

54. Sinha, B.K., et al., *Adriamycin activation and oxygen free radical formation in human breast tumor cells: protective role of glutathione peroxidase in adriamycin resistance.* Cancer Res, 1989. **49**(14): p. 3844-8.

55. Ubezio, P. and F. Civoli, *Flow cytometric detection of hydrogen peroxide production induced by doxorubicin in cancer cells.* Free Radic Biol Med, 1994. **16**(4): p. 509-16.

56. Liu, J., et al., *A therapeutic dose of doxorubicin activates ubiquitin-proteasome system-mediated proteolysis by acting on both the ubiquitination apparatus and proteasome.* Am J Physiol Heart Circ Physiol, 2008. **295**(6): p. H2541-50.

57. Muller, C., et al., *Cellular pharmacokinetics of doxorubicin in patients with chronic lymphocytic leukemia: comparison of bolus administration and continuous infusion.* Cancer Chemother Pharmacol, 1993. **32**(5): p. 379-84.

58. Doroshow, J.H., et al., *Doxorubicin resistance conferred by selective enhancement of intracellular glutathione peroxidase or superoxide dismutase content in human MCF-7 breast cancer cells.* Free Radic Res Commun, 1991. **12-13 Pt 2**: p. 779-81.

59. Martin, E., et al., *Evaluation of the topoisomerase II-inactive bisdioxopiperazine ICRF-161 as a protectant against doxorubicin-induced cardiomyopathy.* Toxicology, 2009. **255**(1-2): p. 72-9.

60. Myers, C., et al., *A randomized controlled trial assessing the prevention of doxorubicin cardiomyopathy by N-acetylcysteine.* Semin Oncol, 1983. **10**(1 Suppl 1): p. 53-5.

61. Li, Y., et al., *Validation of lucigenin (bis-N-methylacridinium) as a chemilumigenic probe for detecting superoxide anion radical production by enzymatic and cellular systems.* J Biol Chem, 1998. **273**(4): p. 2015-23.

62. Li, Y., H. Zhu, and M.A. Trush, *Detection of mitochondria-derived reactive oxygen species production by the chemilumigenic probes lucigenin and luminol.* Biochim Biophys Acta, 1999. **1428**(1): p. 1-12.

63. Li, Y., et al., *Biochemical characterization of lucigenin (Bis-N-methylacridinium) as a chemiluminescent probe for detecting intramitochondrial superoxide anion radical production.* Biochem Biophys Res Commun, 1999. **262**(1): p. 80-7.

64. Li, Y. and M.A. Trush, *Diphenyleneiodonium, an NAD(P)H oxidase inhibitor, also potently inhibits mitochondrial reactive oxygen species production.* Biochem Biophys Res Commun, 1998. **253**(2): p. 295-9.

65. Ruiz-Ramirez, A., et al., *Cytochrome c release from rat liver mitochondria is compromised by increased saturated cardiolipin species induced by sucrose feeding.* Am J Physiol Endocrinol Metab, 2015. **309**(9): p. E777-86.

66. Goormaghtigh, E., et al., *Evidence of a complex between adriamycin derivatives and cardiolipin: Possible role in cardiotoxicity.* Biochemical Pharmacology, 1980. **29**(21): p. 3003-3010.

67. Orrenius, S. and B. Zhivotovsky, *Cardiolipin oxidation sets cytochrome c free.* Nat Chem Biol, 2005. **1**(4): p. 188-9.

68. Baulig, A., et al., *Involvement of reactive oxygen species in the metabolic pathways triggered by diesel exhaust particles in human airway epithelial cells.* Am J Physiol Lung Cell Mol Physiol, 2003. **285**(3): p. L671-9.

69. Suh, N., et al., *A novel synthetic oleanane triterpenoid, 2-cyano-3,12-dioxoolean-1,9-dien-28-oic acid, with potent differentiating, antiproliferative, and anti-inflammatory activity.* Cancer Res, 1999. **59**(2): p. 336-41.

70. Speth, P.A., et al., *Leukemic cell and plasma daunomycin concentrations after bolus injection and 72 h infusion.* Cancer Chemother Pharmacol, 1987. **20**(4): p. 311-5.

71. Benjamin, R.S., C.E. Riggs, Jr., and N.R. Bachur, *Pharmacokinetics and metabolism of adriamycin in man.* Clin Pharmacol Ther, 1973. **14**(4): p. 592-600.

72. Gewirtz, D.A., *A critical evaluation of the mechanisms of action proposed for the antitumor effects of the anthracycline antibiotics adriamycin and daunorubicin.* Biochem Pharmacol, 1999. **57**(7): p. 727-41.

73. Bonavita, F., et al., *H9c2 cardiac myoblasts undergo apoptosis in a model of ischemia consisting of serum deprivation and hypoxia: inhibition by PMA.* FEBS Lett, 2003. **536**(1-3): p. 85-91.

74. Yao, H., et al., *Protection of Luteolin-7-O-Glucoside Against Doxorubicin-Induced Injury Through PTEN/Akt and ERK Pathway in H9c2 Cells.* Cardiovasc Toxicol, 2015.

75. Zordoky, B.N. and A.O. El-Kadi, *H9c2 cell line is a valuable in vitro model to study the drug metabolizing enzymes in the heart.* J Pharmacol Toxicol Methods, 2007. **56**(3): p. 317-22.

76. Mielanczyk, A., et al., *In Vitro Evaluation of Doxorubicin Conjugates Based on Sugar Core Nonlinear Polymethacrylates toward Anticancer Drug Delivery.* Bioconjug Chem, 2016. **27**(4): p. 893-904.

77. Massart, C., et al., *Doxorubicin induces Fas-mediated apoptosis in human thyroid carcinoma cells.* Thyroid, 2004. **14**(4): p. 263-70.

78. Etemad-Moghadam, S., et al., *In vitro study on the effect of doxorubicin on the proliferation markers MCM3 and Ki-67.* J BUON, 2013. **18**(4): p. 1062-8.

79. Dhawan, A., et al., *Aneugenic and clastogenic effects of doxorubicin in human lymphocytes.* Mutagenesis, 2003. **18**(6): p. 487-90.

80. Yang, W., et al., *AMP-activated protein kinase alpha2 and E2F1 transcription factor mediate doxorubicin-induced cytotoxicity by forming a positive signal loop in mouse embryonic fibroblasts and non-carcinoma cells.* J Biol Chem, 2014. **289**(8): p. 4839-52.

81. Serrano, M.J., et al., *Evaluation of a gemcitabine-doxorubicin-paclitaxel combination schedule through flow cytometry assessment of apoptosis extent induced in human breast cancer cell lines.* Jpn J Cancer Res, 2002. **93**(5): p. 559-66.

82. Osman, A.M., et al., *Modulation of doxorubicin cytotoxicity by resveratrol in a human breast cancer cell line.* Cancer Cell Int, 2012. **12**(1): p. 47.

83. Asensio-Lopez, M.C., et al., *Doxorubicin-induced oxidative stress: The protective effect of nicorandil on HL-1 cardiomyocytes.* PLoS One, 2017. **12**(2): p. e0172803.

84. Wang, S., et al., *Doxorubicin induces apoptosis in normal and tumor cells via distinctly different mechanisms. intermediacy of H(2)O(2)- and p53-dependent pathways.* J Biol Chem, 2004. **279**(24): p. 25535-43.

85. Gilliam, L.A., et al., *Doxorubicin acts via mitochondrial ROS to stimulate catabolism in C2C12 myotubes.* Am J Physiol Cell Physiol, 2012. **302**(1): p. C195-202.

86. Kim, S.H., et al., *Doxorubicin-induced platelet procoagulant activities: an important clue for chemotherapy-associated thrombosis.* Toxicol Sci, 2011. **124**(1): p. 215-24.

87. Kim, E.J., et al., *Doxorubicin-induced platelet cytotoxicity: a new contributory factor for doxorubicin-mediated thrombocytopenia.* J Thromb Haemost, 2009. **7**(7): p. 1172-83.

88. Julicher, R.H., et al., *The role of lipid peroxidation in acute doxorubicin-induced cardiotoxicity as studied in rat isolated heart.* J Pharm Pharmacol, 1986. **38**(4): p. 277-82.

89. Demant, E.J. and K. Wassermann, *Doxorubicin induced alterations in lipid metabolism of cultured myocardial cells.* Biochem Pharmacol, 1985. **34**(10): p. 1741-6.

90. Jackson, J.A., et al., *Evaluation of free radical effects and catecholamine alterations in adriamycin cardiotoxicity.* Am J Pathol, 1984. **117**(1): p. 140-53.

91. Ratnam DV, A.D., Bhardwaj V, Sahana DK, Ravikumar MNV, *Role of antioxidants in prophylaxis and therapy: a pharmaceutical perspective.* Journal of controlled release, 2006. **113**: p. 189-207.

92. Michael G, B.R., Kucuk O, Jones DP, *Clinical trials of antioxidants as cancer prevention agents: Past, present, and future.* Free radical biology and medicine 2011. **51** (5): p. 1068-1084.

93. Ratnam, D.V., et al., *Role of antioxidants in prophylaxis and therapy: A pharmaceutical perspective.* J Control Release, 2006. **113**(3): p. 189-207.

94. Kensler, T.W., N. Wakabayashi, and S. Biswal, *Cell survival responses to environmental stresses via the Keap1-Nrf2-ARE pathway.* Annu Rev Pharmacol Toxicol, 2007. **47**: p. 89-116.

95. Singh, A., et al., *Glutathione peroxidase 2, the major cigarette smoke-inducible isoform of GPX in lungs, is regulated by Nrf2.* Am J Respir Cell Mol Biol, 2006. **35**(6): p. 639-50.

96. Kwak, M.K., N. Wakabayashi, and T.W. Kensler, *Chemoprevention through the Keap1-Nrf2 signaling pathway by phase 2 enzyme inducers.* Mutat Res, 2004. **555**(1-2): p. 133-48.

97. Lee, J.M. and J.A. Johnson, *An important role of Nrf2-ARE pathway in the cellular defense mechanism.* J Biochem Mol Biol, 2004. **37**(2): p. 139-43.

98. Kobayashi, M. and M. Yamamoto, *Molecular mechanisms activating the Nrf2-Keap1 pathway of antioxidant gene regulation.* Antioxid Redox Signal, 2005. **7**(3-4): p. 385-94.

99. Itoh, K., et al., *An Nrf2/small Maf heterodimer mediates the induction of phase II detoxifying enzyme genes through antioxidant response elements.* Biochem Biophys Res Commun, 1997. **236**(2): p. 313-22.

100. Dhakshinamoorthy, S., D.J. Long, 2nd, and A.K. Jaiswal, *Antioxidant regulation of genes encoding enzymes that detoxify xenobiotics and carcinogens.* Curr Top Cell Regul, 2000. **36**: p. 201-16.

101. Zhang, H. and H.J. Forman, *Signaling pathways involved in phase II gene induction by alpha, beta-unsaturated aldehydes.* Toxicol Ind Health, 2009. **25**(4-5): p. 269-78.

102. Palmeira, C.M., et al., *Preferential oxidation of cardiac mitochondrial DNA following acute intoxication with doxorubicin.* Biochim Biophys Acta, 1997. **1321**(2): p. 101-6.

103. Serrano, J., et al., *Cardioselective and cumulative oxidation of mitochondrial DNA following subchronic doxorubicin administration.* Biochim Biophys Acta, 1999. **1411**(1): p. 201-5.